Cell

Extensive Promoter-Centered Chromatin Interactions Provide a Topological Basis for Transcription Regulation

Guoliang Li,[1,10] Xiaoan Ruan,[1,10] Raymond K. Auerbach,[2,10] Kuljeet Singh Sandhu,[1,10] Meizhen Zheng,[1] Ping Wang,[1] Huay Mei Poh,[1] Yufen Goh,[1] Joanne Lim,[1] Jingyao Zhang,[1] Hui Shan Sim,[1] Su Qin Peh,[1] Fabianus Hendriyan Mulawadi,[1] Chin Thing Ong,[1] Yuriy L. Orlov,[1] Shuzhen Hong,[1] Zhizhuo Zhang,[3] Steve Landt,[4] Debasish Raha,[4] Ghia Euskirchen,[4] Chia-Lin Wei,[1] Weihong Ge,[5] Huaien Wang,[6] Carrie Davis,[6] Katherine I. Fisher-Aylor,[7] Ali Mortazavi,[7] Mark Gerstein,[2] Thomas Gingeras,[6] Barbara Wold,[7] Yi Sun,[5] Melissa J. Fullwood,[1] Edwin Cheung,[1,8] Edison Liu,[1] Wing-Kin Sung,[1,3] Michael Snyder,[4,*] and Yijun Ruan[1,9,*]

[1]Genome Institute of Singapore, Singapore 138672, Republic of Singapore
[2]Program in Computational Biology and Departments of Molecular, Cellular and Developmental Biology, Yale University, New Haven, CT 06520, USA
[3]Department of Computer Science, School of Computing, National University of Singapore, Singapore 117417, Republic of Singapore
[4]Center for Genomics and Personalized Medicine, Department of Genetics, Stanford University, Stanford, CA 94305, USA
[5]Department of Molecular and Medical Pharmacology, UCLA, Los Angeles, CA 90095, USA
[6]Cold Spring Harbor Laboratory, Cold Spring Harbor, NY 11797, USA
[7]Division of Biology, California Institute of Technology, Pasadena, CA 91125, USA
[8]School of Biological Sciences, Nanyang Technological University, Singapore 637551, Republic of Singapore
[9]College of Life Sciences and Technology, Huazhong Agricultural University, Wuhan 430070, P.R. China
[10]These authors contributed equally to this work
*Correspondence: mpsnyder@stanford.edu (M.S.), ruanyj@gis.a-star.edu.sg (Y.R.)
DOI 10.1016/j.cell.2011.12.014

SUMMARY

Higher-order chromosomal organization for transcription regulation is poorly understood in eukaryotes. Using genome-wide Chromatin Interaction Analysis with Paired-End-Tag sequencing (ChIA-PET), we mapped long-range chromatin interactions associated with RNA polymerase II in human cells and uncovered widespread promoter-centered intragenic, extragenic, and intergenic interactions. These interactions further aggregated into higher-order clusters, wherein proximal and distal genes were engaged through promoter-promoter interactions. Most genes with promoter-promoter interactions were active and transcribed cooperatively, and some interacting promoters could influence each other implying combinatorial complexity of transcriptional controls. Comparative analyses of different cell lines showed that cell-specific chromatin interactions could provide structural frameworks for cell-specific transcription, and suggested significant enrichment of enhancer-promoter interactions for cell-specific functions. Furthermore, genetically-identified disease-associated noncoding elements were found to be spatially engaged with corresponding genes through long-range interactions. Overall, our study provides insights into transcription regulation by three-dimensional chromatin interactions for both housekeeping and cell-specific genes in human cells.

INTRODUCTION

A fundamental question in biology is how genes and regulatory regions are organized and coordinated for transcription regulation. While operons, in which one promoter transcribes multiple genes in a single unit, are common in bacteria (Jacob et al., 1960), and bicistronic transcript structures have been described in worms and flies (Pauli et al., 1988; Zorio et al., 1994), eukaryotic genes are thought to be individually transcribed from their own promoters. However, evidence from in situ fluorescence studies in the last decade suggests that transcription is not evenly distributed and is instead concentrated within large discrete foci in mammalian nuclei, raising the possibility that genes are organized into "transcription factories" (Cook, 1999) containing RNA polymerase II (RNAPII) and other components for transcription. However, this theory lacks evidence with molecular and structural details. Thus, the question of how the regulation of genes is coordinated for transcription in mammalian cells remains largely open.

Mammalian genomes are known to be organized intensively into higher-order conformation inside the micron-sized nuclear space. Consequently, three-dimensional (3D) organization must have a role in the mechanisms for transcription regulation and coordination (Cremer and Cremer, 2001). Chromosome Conformation Capture (3C) and similar techniques (van Steensel and Dekker, 2010) along with traditional in situ techniques have demonstrated that chromatin interactions can regulate

transcriptional and epigenetic states (Cope et al., 2010). However, such analyses are either limited to certain specific domains or of low resolution and lack functional details. Therefore, a global and high-resolution map of functional chromatin interactions is likely to uncover underlying principles of the higher-order genomic architectures regulating transcription.

Recently, we developed Chromatin Interaction Analysis by Paired-End-Tag sequencing (ChIA-PET) for genome-wide investigation of chromatin interactions bound by specific protein factors (Fullwood et al., 2009). By immunoprecipitation of a factor of interest along with associated DNA fragments and followed by diluted proximity ligation of distant DNA fragments tethered together within individual chromatin complexes, we elucidated the association of regulatory information through nonlinear arrangements. We demonstrated that long-range chromatin interactions occur between the transcription factor Estrogen Receptor α (ERα) bound regions and their target promoters. To globally investigate how all active promoters dynamically interact with their corresponding regulatory regions in vivo, we used ChIA-PET to analyze genome-wide chromatin interactions associated with RNAPII. Our results provide insights into the 3D interplay of active promoters as well as regulatory regions and suggest an architectural model in which related genes in mega-base range are organized for efficient and potentially cooperative transcription.

RESULTS

Organizational Complexity of RNAPII-Associated Chromatin Interactions

We analyzed five different human cell lines (MCF7, K562, HeLa, HCT116, and NB4) using ChIA-PET with a RNAPII antibody (8WG16) that recognizes the initiation form of the protein. The cell lines originated from a wide range of lineages, and provided a broad representation of human cells. In our pilot analysis, about 20 million uniquely mapped paired-end reads were generated for each of the ChIA-PET experiments (Table S1A available online), which resulted in two genome-wide datasets: the ChIP-enriched RNAPII binding sites and the RNAPII-bound long-range chromatin interactions. Both intrachromosomal and interchromosomal interaction data were obtained, and the vast majority of chromatin interactions identified by ChIA-PET were intrachromosomal (Table S1B). Twenty-five intrachromosomal and seven interchromosomal interactions were validated either by 3C, DNA-FISH, or both (Figure S1 and inset of Figure 1C).

To present an inclusive view of the RNAPII-associated human chromatin interactome, we combined the ChIA-PET sequence reads from the six pilot experiments into one dataset for analysis (Table S1). Using embedded nucleotide barcode controls and statistical analyses, we assessed the data quality, filtered out the technical noise, and identified high-confidence binding sites and interacting PET clusters (Experimental Procedures). From the combined pilot dataset, we identified 14,604 high-confidence (FDR < 0.05) RNAPII binding sites as well as 19,856 high-confidence intrachromosomal interaction PET clusters (Table S3). The majority (83%) of RNAPII binding sites in the combined dataset were proximal to 5′ Transcription Start Sites (TSS) of genes (Figure 1A). There were also distinct but relatively weaker enrichments of peaks at the 3′ Transcription End Sites (TES) of genes. Similar patterns were seen in all the individual experiments. Of the total RNAPII binding sites, 9,487 (65%) were involved in chromatin interactions and these sites showed higher RNAPII occupancy than those not involved in interactions (Figure 1B), indicating that most highly-enriched RNAPII binding sites are involved in looped chromatin conformations.

Three basic types of interactions were identified around gene promoters in the combined pilot dataset: intragenic (promoter to gene internal regions, 938, 5%), extragenic (promoter to distal regulatory elements such as enhancer, 6,530, 33%), and intergenic (promoter-promoter of different genes, 8,282, 42%). There was also a subcategory composed of intermediate enhancer-enhancer interactions (4,106, 20%). Some interactions (2,341, 12%) were standalone duplex interactions between two interacting anchor regions, whereas most (17,515, 88%) were further aggregated into 1,544 interaction complexes.

We speculated that the isolated RNAPII binding at promoter sites, which are not involved in interactions, may reflect the basal promoter function for gene transcription, and thus were termed "basal promoters." By contrast, RNAPII-associated interactions might constitute a structural basis for complex regulatory mechanisms. These basic interactions further aggregated into complex architectures which we classified as "single-gene" or "multigene" complexes depending on the number of genes involved (Figure 1C). The single-gene models consisted of single or multiple enhancer interactions with only one gene promoter, whereas the multigene models included intergenic promoter-promoter interactions and could also include intragenic and extragenic enhancer-promoter interactions. Moreover, several such complexes, distantly separated on a chromosome or on different chromosomes, further converged to form higher-order multigene interaction complexes (Figures S1B, S1D, S1F, and S1G). Many chromatin complexes had genomic spans of 150 kb–200 kb, and a few complexes spanned several megabases. Although there were only 1,328 multigene complexes in this combined pilot dataset, 11,723 genes were engaged in these complexes for an average of 8.8 genes per interaction complex (Figure 1D), indicating that promoter-promoter interactions were widespread and may play a significant role in transcription regulation.

To understand how these looping structures influence transcription, we characterized these RNAPII-associated chromatin models (basal promoters, single-gene and multigene complexes) for structural features (genomic property), functional output (transcription activity), and epigenomic marks (chromatin state).

Distinct Genomic Properties of Single- and Multigene Interaction Models

To determine the genomic characteristics of RNAPII-associated chromatin structures, we mapped several genomic descriptors that were known to associate with the expressivity of the human genome (Versteeg et al., 2003), including GC content, gene density, SINE/LINE density, gene length, and the intron/exon ratio. In our analyses (Figure 2, Figure S2A), the multigene complexes were significantly enriched with higher GC content, higher gene and SINE density, and lower LINE density as

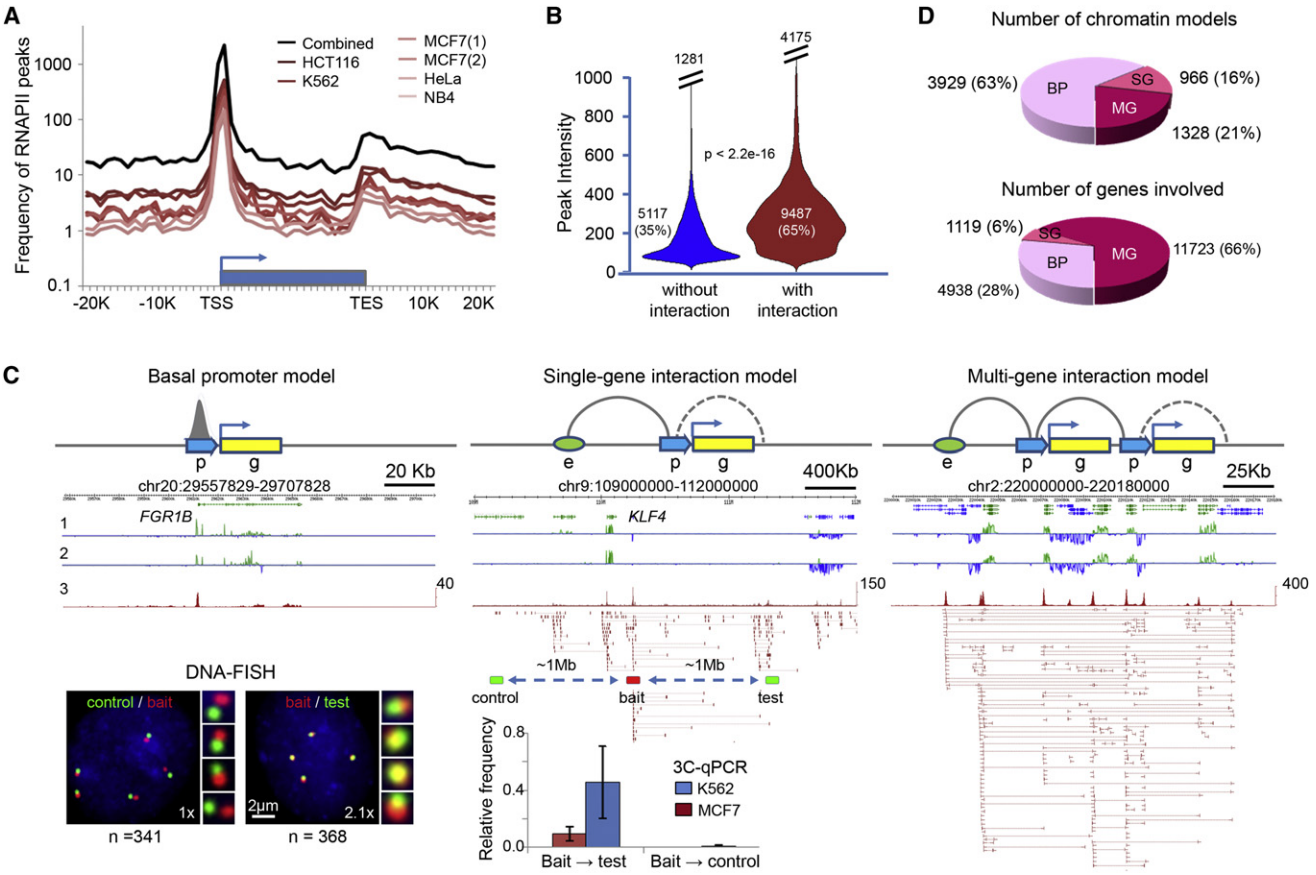

Figure 1. Characterization of RNAPII Binding Peaks and Chromatin Interactions

(A) RNAPII binding profile around gene body.

(B) Violin plots for intensities of RNAPII peaks involved (red, mean intensity = 281) and not involved in interactions (blue, mean intensity = 141).

(C) RNAPII-associated chromatin models: basal promoter (BP) with RNAPII binding but no chromatin interaction, single-gene (SG) complex with intra- and/or extragenic interactions and multigene (MG) complex with multiple genes in the interaction clusters. p, promoter; g, gene; and e, enhancer. The dotted curve for possible intragenic loop, and the solid curve for potential loop of enhancer-promoter and promoter-promoter interactions. Data tracks are: 1 and 2, strand specific RNA-Seq data of MCF7 and K562; 3, RNAPII binding peaks and ChIA-PET data. Inset (bottom): DNA-FISH and 3C-qPCR validations of the extragenic interaction at the *KLF4* locus, where the *KLF4* promoter and enhancer are ~1 Mb apart. Genomic locations used for 3C bait, test and control sites are indicated. The same locations were also used for DNA-FISH. The numbers (n) of nuclei counted and the fold change (x) in the number of instances showing close proximity ($\leq$1 μm) are indicated. 3C-qPCR mean values and standard error of means (SEM) from three independent experiments are shown.

(D) Distribution of chromatin models (BP, SG, MG) and the numbers of genes engaged in the models.

See also Figure S1, Table S1, Table S2, and Table S3.

compared to the single-gene interaction complexes and the regions of basal promoters, suggesting that multigene complexes were located in open chromatin and highly transcribed regions. In addition, genes in the multigene complex regions were relatively shorter than other gene categories, which is yet another property of highly expressed genes (Eisenberg and Levanon, 2003). Conversely, genomic loci associated with the single-gene complexes lay in the regions with lower gene and SINE density. Moreover, the genes engaged in the single-gene complexes were significantly longer and had higher intron/exon ratios than the genes of other chromatin models (Figure 2B). These observations suggest that genes with enhancer-promoter interactions in single-gene complexes were more likely to be tissue-specific or developmentally regulated, in line with the previous findings that genes in gene-poor regions associated with several distant regulatory elements, tended to be longer and had a higher noncoding to coding ratio than housekeeping genes (Eisenberg and Levanon, 2003; Taylor, 2005).

Interacting Genes Show Correlated Expression

To investigate the functional output of genes involved in the different chromatin models, as defined by transcriptional activity, we focused our analyses on MCF7 cells, as it is a well-characterized human cancer cell model with complementary datasets including RNA-Seq (Experimental Procedures), time-course microarray gene expression (Fullwood et al., 2009), and GRO-Seq datasets (Hah et al., 2011).

Consistent with the combined pilot dataset, 90% binding sites in MCF7 cells were found proximal to known gene promoters and 97% genes with RNAPII present at their promoters had

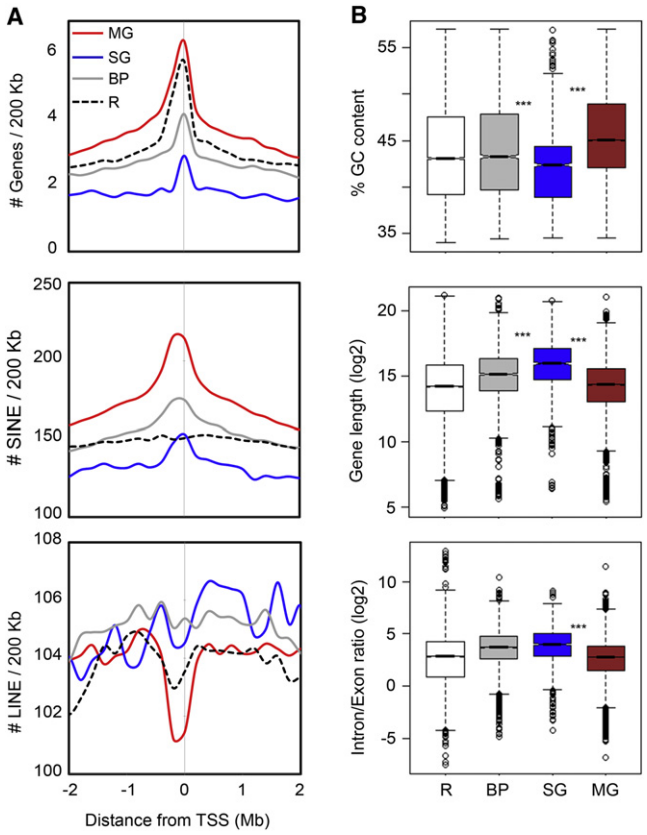

Figure 2. Genomic Properties of Promoter-Centered Chromatin Models

(A) Aggregation plots showing enrichment of genes, SINE and LINE elements around the TSS of genes in different chromatin models. Unique RefSeq TSSs were used for analyses. Red curve stands for multigene (MG) model, blue for single-gene (SG) model, gray for basal promoter (BP) model, and black dotted line for the rest of the genes (R).

(B) Box-plots showing distribution of percentage GC content of GC isochore around different models, gene length, and intron/exon ratio of RefSeq genes involved in the models. Triple asterisks (***) signifies p value < 2.2E-16. Red box stands for MG, blue for SG, and gray for BP. Open box is for R (rest of genic regions) as background.

See also Figure S2.

detectable transcriptional activity by RNA-Seq (Figure 3A). The interactive RNAPII binding sites that were distal to gene promoters included intra- and extragenic regulatory elements such as enhancers. Approximately 45% of the extragenic distal regulatory sites had detectable RNA signals that could represent possible noncoding RNA (ncRNA) transcripts.

For genes associated with the three chromatin models, we analyzed the transcription levels measured by RNA-Seq reads. As shown in Figure 3B, in general, RNAPII binding at promoter sites correlated well with the expression level of the corresponding genes. Interestingly, the genes involved in the single-gene and the multigene models showed higher correlation between RNAPII binding and RNA-Seq signal (Pearson's correlation coefficient: PCC: 0.46 and 0.45 respectively) as compared to basal promoter genes (PCC: 0.24). Moreover, we observed that genes linked by complex chromatin interactions, especially those in multigene complexes, had significantly higher expression levels than basal promoter genes (Figure 3C). This high expression appeared to be limited to genes interacting at the RNAPII anchor sites, as compared to genes located in the intervening chromatin loops. These data indicated that promoter-promoter interactions in multigene complexes were associated with higher transcriptional activity, which is consistent with our observations of their associated genomic features.

Next, we characterized the expression patterns of genes present in the interacting regions using microarray data derived from 84 human tissues (Su et al., 2002). We found distinct representation of tissue-specific and housekeeping genes in the three chromatin models (Figure 3D, Figures S3A and S3B). Most genes in single-gene complexes with enhancer-promoter connectivity were tissue-specific, consistent with growing evidence that the expression levels of developmental and tissue-specific genes are largely modulated through *cis*-remote regulatory elements and *trans*-protein factors (Hou et al., 2010; Schoenfelder et al., 2010), and consistent with their genomic features (less gene density, longer gene body and higher intron/exon ratio) as previously described. Conversely, genes involved in multigene complexes as well as the basal promoter genes were characterized as both tissue-specific and housekeeping categories. These observations were also supported by normalized CpG content and GC-skew at their promoter regions (Figures S3C and S3D).

As promoter-promoter interactions cluster multiple genes, they could provide an ideal topological framework for potential transcriptional coordination of both tissue-specific and housekeeping genes. This observation agrees with the evidence that "ridges," which are domains of highly transcribed genes, contain both housekeeping and tissue-specific genes (Versteeg et al., 2003). Since large numbers of genes are found in multigene complexes, we propose that promoter-promoter interactions could serve as a dominant mechanism for transcription regulation of both housekeeping and tissue-specific genes in mammalian genomes.

Next, we sought to determine whether genes with promoter-promoter interactions were more likely to be transcriptionally coordinated. RNA-Seq data showed that most of the paired genes with promoter-promoter interactions were expressed together at high levels (Figure 3E; Figure S3E). To further assess the coordinated transcription of paired genes across different conditions, we performed Pearson's correlation analysis using estrogen-induced time course of GRO-Seq data (Hah et al., 2011) that measured transcription initiation rates of estrogen responsive genes, and observed significant transcriptional correlation (Figure 3F; p value < 2.2E-16). Interestingly, the correlation was even greater for ERα-mediated gene pairs derived from our earlier data (Fullwood et al., 2009), suggesting stronger correlation of transcription for genes involved in multigene complexes mediated by specific transcription factors. Similar correlation was also observed from other gene expression datasets (Figures S3F–S3I). As expected, housekeeping genes and genes belonging to the same GO classes showed even higher correlation than the rest (Figures S3J and S3K). Altogether, our analyses indicated that a significant proportion of gene pairs

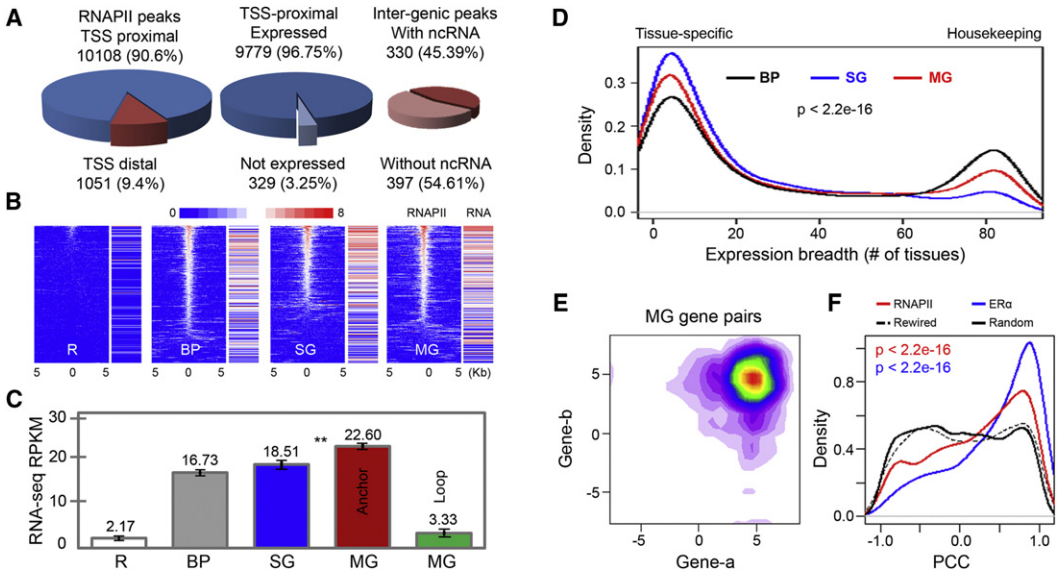

Figure 3. Transcriptional Activities in RNAPII-Associated Chromatin Models in MCF7 Cells

(A) Pie charts of RNAPII binding peaks proximal (blue) or distal (red) to TSS of genes (left), RNA-Seq data for genes with RNAPII peaks near TSS (middle), and RNA-Seq enrichment around intergenic RNAPII peaks (right).

(B) Correlation of RNAPII binding in basal promoter (BP), single-gene (SG) and multigene (MG) models with gene transcription levels measured by RNA-Seq. The RNAPII enrichment heatmap shows binding intensity centered on TSS (±5 kb) along with corresponding gene transcription intensity.

(C) Bar plots of expression levels of genes in the three models (BP, SG, and MG). RNA-Seq mean values (RPKM) and standard error of means (SEM) from genes in the corresponding models are shown. MG complexes also contain "anchor genes" (TSS proximal to interacting anchors) and "loop genes" (distant from anchors, residing in loop regions). The remaining genes (R) not bound by RNAPII were included as a control. Double asterisks (**) indicate significant differences between the mean expressions of genes from SG and MG models (p value < 4.02E-08).

(D) Expression breadth (number of tissues a gene is expressed in) of genes present in three different chromatin models. P value is calculated using the nonparametric test of Kruskal-Wallis.

(E) Contour plot of log-transformed RNA-Seq RPKM values for cotranscription of interacting genes involved in MG models in MCF7 cells.

(F) Distribution of PCC values for RNAPII- and ERα-bound interacting gene pairs, randomly rewired gene pairs, and randomly picked gene pairs from control regions with the same genomic span and gene density distribution as the multigene complex regions.

See also Figure S3.

involved in promoter-promoter interactions tended to be transcribed cooperatively.

Multigene Complexes Provide Structural Framework for Cotranscription

Correlated expression of interacting genes suggests that the multigene interaction complex might provide a molecular basis for the postulated "transcription factory" (Cook, 1999). To elucidate the link between the multigene complexes revealed by ChIA-PET and transcription factories, we performed 3D DNA-FISH experiments using probes representing distinct multigene complexes in combination with RNAPII-IF staining in MCF7 nuclei (Experimental Procedures). All experiments on four genomic loci randomly chosen from multigene complexes revealed a significant association of the multigene complex loci with RNAPII foci (Figure 4A-B), adding further evidence to support our view that multigene complexes could provide a structural framework for cotranscription.

Furthermore, gene families were significantly over-represented (p value < 0.006) in the multigene complexes (Figure S3L), such as *HIST*, *ZNF*, *KRT*, *HOXC*, etc. (Table S4). Taking the *HIST1H* family as an example, the 58 genes of this family located on chromosome 6 formed three multigene complexes, and these three complexes converged into a higher-order super-complex, suggesting that all *HIST1H* genes were organized in a single chromatin architecture for coordinated transcription (Figure 4C). All *HIST1H* genes were actively transcribed in both MCF7 and K562 cells, and were highly coregulated across different tissues and cellular conditions (Figure 4D). Interestingly, *HFE*, a gene was not a part of the *HIST1H* family but was located in the middle of the first *HIST1H* multigene complex, was not anchored at the interaction sites and was not expressed. Similarly, the genes located in the intervening loop regions between the three *HIST1H* interacting complexes were relatively less active and much less coordinated for coregulation across different tissues and cellular conditions. This case exemplifies the model where multigene complexes organize genes with similar functions across genomic space for coordinated expression.

Multigene Complexes Support Synergistic Transcription Regulation

To further investigate the likelihood that the multigene complex structure might provide a topological framework for transcriptional coregulation of interacting genes involved in such topology, we designed a set of perturbation experiments to

test this. After comparing the RNAPII and ERα ChIA-PET data from MCF7 cells, we found that the RNAPII-bound multigene complex at the *GREB1* locus partially overlaps with the ERα-bound chromatin loops, suggesting that this interaction complex, in part, is associated with ERα. Therefore, we performed siRNA experiments to knockdown the protein level of ERα in MCF7 cells, and monitored the alteration of chromatin interactions and gene transcription in the *GREB1* multigene complex. Several chromatin interaction loops at this locus were disrupted by siERα transfection as tested by 3C experiments (Figure 4E). In addition to *GREB1,* which had a strong response to estrogen induction and reduction by siERα knockdown (Figures S4A–S4D), we observed that the other genes in this complex such as *E2F6*, *KCNF1* and *ATP6VC12* also had various levels of response to induction by estrogen and reduction by siERα knockdown (Figure 4F). Interestingly, these genes did not directly interact with ERα at their promoter regions, but indirectly associated with ERα through RNAPII-bound chromatin loops. As a control, this effect was not seen in the nearby genes such as *NOL10* and *HPCAL1* that were in other RNAPII interaction complexes and also did not interact with ERα (Figure 4G). Similar results were observed at another interaction locus centered on the *GPR68* and *CCDC88C* genes (Figure S4E). Thus, these results indicate that a specific stimulus (estrogen) could lead to coactivation of genes organized primarily through RNAPII-bound multigene complexes, and perturbation at one gene locus (loss of ERα binding in this case) in a multigene complex could alter the transcriptional states of other interacting genes within the same complex. Although genes in close genomic distances with each other had been reported to be correlated in expression levels (Singer et al., 2005), our data suggests that the conjoint expression can be mediated through chromatin interactions. The functional significance of such coregulation needs further investigation.

Epigenomic Marks Associated with Chromatin Interaction Sites

To study the association of transcription factors (TFs) with the RNAPII interactions, we examined the enrichment of 20 different TFs in K562 cells at the RNAPII interaction sites from the three chromatin models in our K562 ChIA-PET dataset (Figures 5A and 5B, Figures S5A–S5D). General TFs such as E2F4 and E2F6 (Figure 5A, Figure S5A) directly bound at TSS sites (Figure 5B for a specific example). By contrast, specific TFs such as JunD and Max preferentially bound to distal regulatory sites and marked potential enhancers (Figure S5B). Several chromatin remodeling factors and chromatin organization proteins such as INI1, BRG1, CTCF, and RAD21 associated primarily with non-TSS sites, suggesting that they may mediate long-range interactions with enhancer regions (Figure 5A, Figure S5C). This hypothesis is consistent with other observations that INI1 and BRG1, two subunits of the SWI/SNF complex, were involved in transcriptional looping (Euskirchen et al., 2011). A common observation among all the factors was that interaction sites in the multigene complexes consistently showed elevated levels of factor enrichment, suggesting that the cooperative binding of factors in gene-rich domains leads to higher transcriptional activity, or these transcriptionally active open chromatin domains might converge to distinct specialized transcription factories, each enriched with general and specific TFs.

We further explored the histone modification data available from the ENCODE Consortium. Collectively, we found high enrichment of active histone modification marks coupled with a lack of repressive marks in RNAPII interaction sites, confirming that the RNAPII interaction sites mapped by our ChIA-PET data were located in promoter and distal regulatory regions engaged and/or poised for high transcription levels (Figure S5D). Interestingly, the enrichment of active marks was highest in the multigene complexes, indicating that these might constitute transcriptional hubs. Our observations matched previous findings that the enrichment of active histone modifications positively correlated with RNAPII occupancy (Barski et al., 2007).

We observed similar histone modification profiles in MCF7 cells (Figure 5C) using data that we generated previously (Joseph et al., 2010). In particular, we applied the log ratio of H3K4me3/H3K4me1 signal as a quantitative measurement of the likelihood that a genomic locus can act as a promoter or enhancer. Most noninteracting RNAPII sites proximal to TSS in basal promoter model showed high log ratios (Figure 5D, plot 1; median = 2.4; > 90% of the binding regions have log ratios > 0), whereas most of the RNAPII interaction sites distal to TSS in the single-gene complex model and the multigene complex model (conventional enhancer sites) showed low H3K4me3/me1 log ratios (Figure 5D, plot 4 and 6; median < −0.72), confirming that this log ratio could reflect relative capacities of promoters and enhancers. Surprisingly, examination of RNAPII interaction sites proximal to known TSSs in the multigene complexes (Figure 5D plot 5) revealed two peaks in the histogram of the log ratios, suggesting a mixture of enhancer and promoter elements in the promoter regions. Detailed profiles of H3K4me3 and H3K4me1 marks around the center (±5 kb) of those RNAPII interaction sites showed distinct characteristics of promoter-like, enhancer-like sub-groups (Figure 5D, heatmap). Moreover, enhancer-like RNAPII interaction sites, on average, showed lower transcriptional activity than the promoter-like RNAPII sites (Figure S5J). Thus, a large portion of interacting promoters may also have potential enhancer functions. We observed the same inverse correlation of H3K4me3/me1 log ratio at the TSS proximal and TSS distal RNAPII sites for K562 (Figure 5A), indicating that this observation is a general phenomenon applicable to all cell types.

Interacting Promoters Possess Combinatorial Regulatory Functions

To examine potential enhancer activity of promoters, we performed luciferase reporter gene assays, a commonly used method for promoter and enhancer characterization (Pan et al., 2008). In these assays, approximately 500 bp fragments of the expected promoter regions were cloned upstream of a luciferase reporter gene construct either in a proximal position as the driving promoter or in a distal position as a presumed enhancer, and the constructs were transfected into MCF7 cells (Experimental Procedures, Figures S5E–S5I). As shown in Figure 5E, the two interacting loci *INTS1* and *MAFK* were 26 kb apart, and our RNA-Seq data suggested that both genes were active

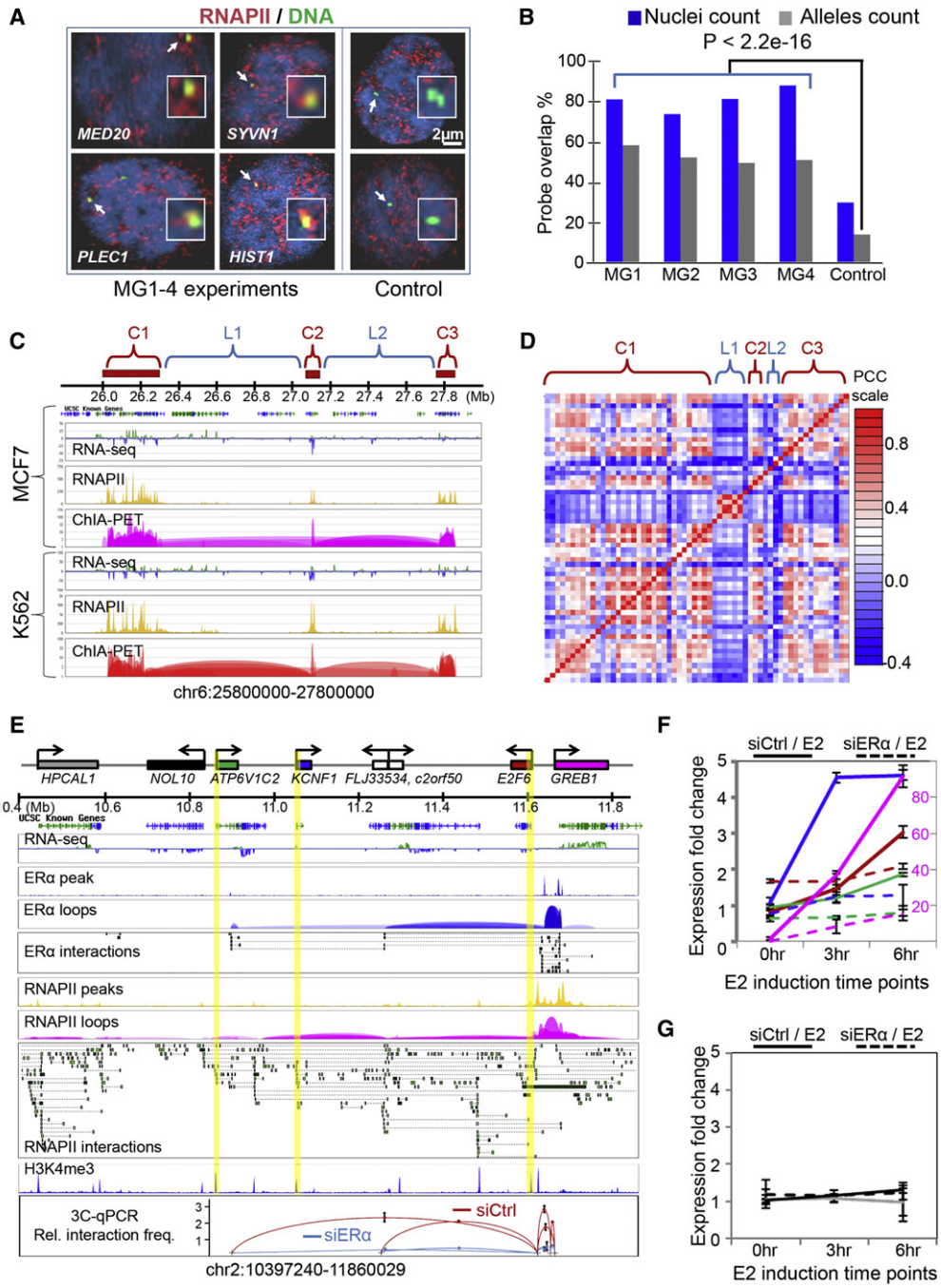

Figure 4. Transcriptional Coordination in Multigene Chromatin Complexes

(A) Colocalization of multigene loci with RNAPII foci. Shown are the nuclear images of RNAPII IF-staining with four randomly-selected multigene loci (MG1-4) and 2 control loci. Representative gene loci are *MED20*, *SYVN1*, *HIST1*, and *PLEC1*.

(B) Quantitative analysis of nuclei (n = 476) and alleles showing overlap of MG loci and RNAPII foci. Percentage overlaps from MG loci and those from control loci are significantly different.

(C) Super multigene complex of the histone gene family. Three distant clusters (C1, C2, C3) of *HIST1H* genes converge together in a super-MG complex. Shown are RNA-Seq, RNAPII and ChIA-PET tracks in MCF7 and K562 cells.

(D) Cotranscription of *HIST1H* genes in the super-MG complex in (C). Correlation matrix derived from publicly available microarray data of 4,787 samples (Supplemental Information). The rows and columns correspond to genes in each complex and the intervening regions.

(E) RNAPII-bound multigene complex at the *GREB1* locus. Shown are the ERα- and RNAPII-bound chromatin interactions. Highlighted promoters are anchored by RNAPII, but not by ERα. The bottom panel shows relative interaction frequency by 3C-qPCR data for the perturbation experiments using siERα knockdown and estrogen induction.

in MCF7 cells. However, the normalized log ratio of H3K4me3/me1 was 0.36 for the *INTS1* promoter and 1.13 for the *MAFK* promoter, suggesting that the *INTS1* promoter may have enhancer properties. To test this, we cloned the *INTS1* promoter fragment in both orientations upstream of the *MAFK* promoter flanking the luciferase gene. The luciferase reporter gene assay showed at least 7-fold enhancement of luciferase expression from the *MAFK* promoter activity by the *INTS1* promoter fragment, indicating that a bona fide promoter can act as an enhancer to augment the activities of other promoters.

In another example (Figure 5F), the promoter of *CALM1* interacts with an enhancer element 15 kb upstream and connects to the promoter of *C14orf102* further upstream in 65 kb. Both RNA-Seq data and the H3K4me3/me1 log ratio indicated that the *CALM1* promoter was strong, whereas the *C14orf102* promoter was weak and enhancer-like. The luciferase reporter gene assay showed marginal enhancement to the *CALM1* promoter reporter gene activity by the native *CALM1* enhancer and the *C14orf102* promoter individually. However, the combined *CALM1* enhancer and the *C14orf102* promoter together led to a significant ~3-fold enhancement of reporter expression from the *CALM1* promoter. This result further validates the enhancer function by interacting promoters and elucidates a possibility of combinatorial effect among interacting elements in multigene interaction complexes for transcription regulation.

Next, we asked whether promoters with enhancer activity act specifically on their target genes. We swapped the promoter elements in the two examples of *INTS1*-to-*MAFK* and *C14orf102*-to-*CALM1* for additional reporter genes assays (Figure 5G). Intriguingly, when placed upstream to the *CALM1* promoter, the *INTS1* promoter showed remarkable enhancement of *CALM1* promoter activity. Similarly, the combined construct of *C14orf102* promoter and *CALM1* enhancer also increased *MAFK* promoter activity significantly. Meanwhile, a TATA box deleted promoter and other control promoters (either active or inactive), taken from the nearby genes that are not involved in a promoter-promoter relationship, did not show cooperative enhancement to *MAFK* and *CALM1* promoter activities (Figures S5H and S5I). Thus, these results suggest a common property for promoters with enhancer capacity that could influence other promoters.

In addition, we also tested the combination of inserting the enhancer-like promoter fragment in the position proximal to luciferase gene and the strong promoter in the distal position in the reporter gene construct. Of the 20 such luciferase experiments, we observed that the weaker promoters conveyed significant enhancer function to their stronger interacting partners in luciferase activity rather than the reverse (Figure S5K). In the case of interacting pair *INTS1* (enhancer-like promoter) and *MAFK* (strong promoter), the strong promoter *MAFK* did not demonstrate significant enhancer activity (Figure S5L). Thus, at promoter sites, there is an inverse relationship between enhancer and promoter functions.

Cell-Line Specificity of Long-Range Chromatin Interactions

To elucidate the cell-line specificity of chromatin interactions, we saturated the coverage of chromatin interactions through deep sequencing of more MCF7 and K562 ChIA-PET replicates (Experimental Procedures). The saturated libraries are highly reproducible for interactions, and thus highly reliable for intercell line comparative analysis. These libraries exhibit the same pattern of genomic descriptors as the pilot libraries (Figures S2B and S2C). With comprehensive ChIA-PET and RNA-Seq datasets, we performed comparative analysis between the two cell lines and identified cell-line specific genes and chromatin interactions (Figure 6A). Most of the genes specifically expressed in their respective cells also showed cell-specific interactions (Figure 6B), implying that cell-specific chromatin interactions provide the structural basis for cell-specific transcription. Gene Ontology (GO) analysis revealed significant enrichment of erythroid related GO terms such as response to stimulus and blood circulation for genes with specific expression and chromatin interactions in K562 cells, whereas GO terms such as ectoderm development and related biological process were enriched in MCF7 cells (Figure 6C, Figure S6A). As expected, the genes common in both cell lines showed enrichment of housekeeping functions like metabolism, cell-cycle and signal transduction (Figure S6B).

Among the chromatin interactions specific to K562 cells, we captured many previously characterized interactions including the α- and β-globin loci (Bau et al., 2011; Hou et al., 2010). Figure 6D shows extensive interactions identified by ChIA-PET data between the α-globin gene locus and the DNase hypersensitive (DHS) sites present in the gene body of the *C16orf35* gene. Additionally, we found that the α-globin locus in K562 extended its interactions to the neighboring domains, which were constitutively active in both K562 and MCF7 cells, whereas the interactions to α-globin genes are K562-specific, suggesting a complex chromatin architecture for spatiotemporal regulation of both constitutive and cell-specific transcription. Similarly, the β-globin gene locus also displayed previously known K562-specific interactions with the nearby locus control region (Figure S6C).

GREB1 is a well characterized MCF7-specific gene. As expected, we found abundant chromatin interactions associated with RNAPII at this locus in MCF7, but not in K562 cells (Figure 6E). In addition to recapitulating the previously identified ERα-associated interactions (Fullwood et al., 2009), RNAPII interaction data showed an additional interaction site on the far most upstream (left in Figure 6E) side of this complex. A strong H3K4me1 mark on this site suggested that this is potentially an enhancer site for a transcription factor other than ERα.

(F and G) Time course RT-qPCR following estrogen (E2) induction after siControl (solid) and siERα (dashed) transfections of MCF7 cells. Colors of the curves correspond to genes shown in (E). A secondary axis (red, right side) is used for *GREB1* expression to accommodate its high expression level. Expression data of genes involved in the *GREB1* multigene complex are in (F), and the data for genes outside of the complex are in (G). RT-qPCR mean values and standard deviations (SD) from two independent experiments are shown.
See also Figure S4 and Table S2.

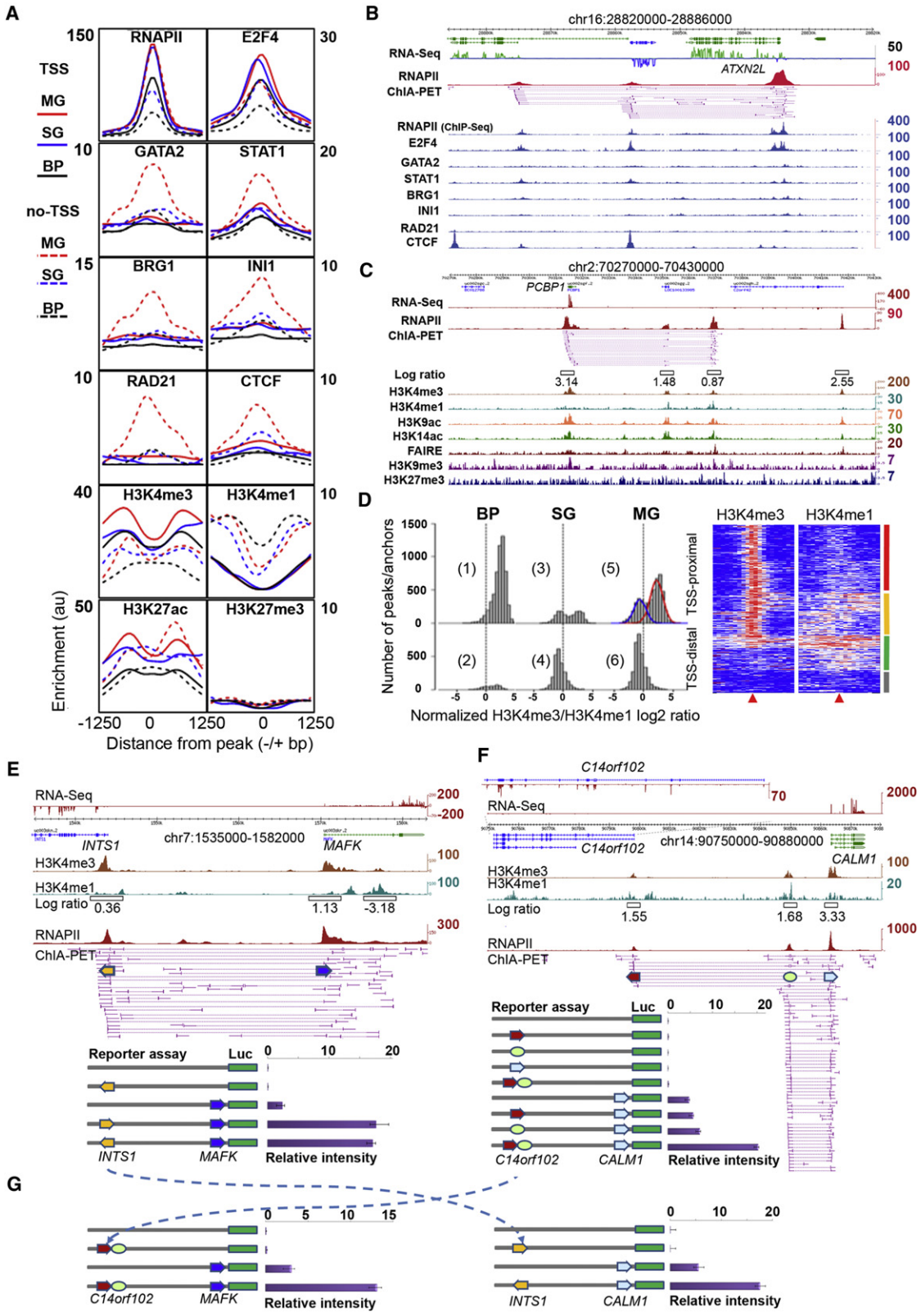
A
RNAPII
E2F4
GATA2
STAT1
BRG1
INI1
RAD21
CTCF
H3K4me3
H3K4me1
H3K27ac
H3K27me3
TSS
MG
SG
BP
no-TSS
Enrichment (au)
-1250 0 1250 0 1250
Distance from peak (-/+ bp)
B
chr16:28820000-28886000
RNA-Seq
RNAPII ChIA-PET
ATXN2L
RNAPII (ChIP-Seq)
E2F4
GATA2
STAT1
BRG1
INI1
RAD21
CTCF
C
chr2:70270000-70430000
PCBP1
RNA-Seq
RNAPII ChIA-PET
Log ratio
3.14
1.48
0.87
2.55
H3K4me3
H3K4me1
H3K9ac
H3K14ac
FAIRE
H3K9me3
H3K27me3
D
BP
SG
MG
H3K4me3
H3K4me1
Number of peaks/anchors
TSS-proximal
TSS-distal
Normalized H3K4me3/H3K4me1 log2 ratio
E
RNA-Seq
chr7:1535000-1582000
INTS1
MAFK
H3K4me3
H3K4me1
Log ratio
0.36
1.13
-3.18
RNAPII ChIA-PET
Reporter assay
Luc
Relative intensity
F
C14orf102
RNA-Seq
chr14:90750000-90880000
CALM1
H3K4me3
H3K4me1
Log ratio
1.55
1.68
3.33
RNAPII ChIA-PET
Reporter assay
Luc
Relative intensity
G
C14orf102
MAFK
INTS1
CALM1
Relative intensity

Intriguingly, a significant RNA-Seq peak was also identified at this site, indicating a possible enhancer RNA transcript, a new class of noncoding RNA species (Kim et al., 2010).

Long-Range Enhancer-Promoter Interactions and Disease-Associated Noncoding Elements

Our data showed that the enhancer-promoter interactions were significantly enriched over other types of interactions for cell-specific genes (Figure 7A) when compared to genes commonly expressed in both cell lines. This finding supported the general view that distant-acting enhancers tend to be specifically involved in tissue-specific genes, and was consistent with our analysis in Figure 3D. Although potential enhancer sites can be identified using high throughput approaches (Heintzman et al., 2009), it is still challenging to connect enhancers to their target genes that are hundreds of kilobases away. Moreover, many remote enhancers could be embedded in intronic regions of other distantly located genes (Visel et al., 2009), making it notoriously difficult to relate enhancers to their specific target genes. In this study, we identified tens of thousands enhancer-promoter interactions (Table S1C) including approximately 1000 ultra-long-distance (500 kb to megabases) events. We observed that $\geq$ 40% of enhancers do not interact with their nearest promoters and instead jump over to their target promoters, bypassing several intervening genes (Figure 7B, Figure S7).

An interesting example is the *SHH* gene that was expressed in MCF7 but not in K562 cells (Figure 7C). *SHH* is important in development and related to certain cancers (Lettice et al., 2002). Transcription of *SHH* is controlled by its enhancer which is located 1 Mb away and embedded in the intronic region of *LMBR1*; point mutation in this enhancer site is known to cause *preaxial polydactyly,* a common congenital limb malformation in mammals (Lettice et al., 2002). We found abundant interaction data between the *SHH* promoter and the previously characterized *SHH* enhancer site in the *LMBR1* intronic region in MCF7 cells, but no interaction data in K562 cells (Figure 7C), which correlated well with their *SHH* transcription status. This is consistent with earlier observations (Amano et al., 2009).

In another interesting example, we identified two major interaction sites located ~600 kb and ~1 Mb downstream from the *IRS1* gene promoter. IRS1 is known to participate in type-2 diabetes (T2D) mellitus, and is found specifically expressed in MCF7 cells (Figure 7D). A recent GWAS study uncovered a cluster of SNPs that is genetically associated with high risk to insulin resistance, T2D, and coronary artery heart disease (Kilpelainen et al., 2011). This high risk locus is found located in one of the *IRS1* enhancer sites (Figure 7D). Thus, our data provides experimental evidence to suggest that this disease-risk locus could be physically connected with the *IRS1* promoter, potentially serving as a critical long-range enhancer to regulate the expression of *IRS1*, in a similar manner as the *SHH* locus. Other examples of long-range and cell-specific enhancer-promoter interactions in MCF7 and K562 are shown in Figure S7. Taken together, these results suggest that ChIA-PET interaction data may better inform the association of a SNP with a gene involved in a disease process by providing evidence for direct physical interactions.

DISCUSSION

Through genome-wide mapping, we comprehensively analyzed RNAPII-associated long-range chromatin interactions. Our most interesting finding was the extensive promoter-promoter interactions among proximal and distant genes from 5 human cell-lines, which indicated that this mechanism is common in cells. Our work with reporter gene and siRNA knockdown assays provided experimental evidence that many promoters in the multigene complexes can cooperatively regulate the activity of other promoters with which they interact. Our observations thus blurred the conventional definition of promoter and regulatory elements for transcription. With such promoter-promoter interactions, we speculate that genetic error at one particular promoter might also propagate to other promoters and hence could lead to pleiotropic consequences depending on the interaction network within a cell type. Intriguingly, the multigene complexes illustrated in this study are, in principle, akin to the

Figure 5. Epigenomic Profiles of Chromatin Interactions and Combinatorial Regulation of Interacting Promoters

(A) Enrichment profiles of TFs and histone modifications centered on RNAPII peaks (±1250 bp) of interacting loci of the three models in K562 cells. Solid lines represent "TSS" proximal regions and dotted lines depict "non-TSS" regions. y axis: sliding median for ChIP-Seq enrichment in the region.

(B) Examples of TF enrichment at RNAPII interacting loci in K562 cells.

(C) Histone modification marks and open chromatin mark (FAIRE) associated with chromatin interaction sites in MCF7 cells. The width of the open boxes in the log ratio track reflects the region where the H3K4me3 and H3K4me1 data were used for the log ratio calculation.

(D) Histograms of normalized H3K4me3/me1 log ratio at RNAPII sites proximal to TSS (TSS) and distal to TSS (non-TSS) of genes in the three chromatin models in MCF7 cells. Two peaks are seen in plot #5 (blue curve for enhancer-like, and the red for promoter-like). The heatmap shows detailed H3K4me3 and H3K4me1 enrichments around RNAPII interaction sites (±5 kb) proximal to TSS. Four distinct clusters of RNAPII sites are promoter-like (red), enhancer-like (green), heterogeneous (yellow) and weak signals (gray).

(E–G) Reporter gene assay of interacting promoters in MCF7 cells. RNA-Seq, H3K4me3, H3K4me1, H3K4me3/me1 ratio, and RNAPII ChIA-PET data tracks are shown. Numbers on the right side for each track indicate the highest peak intensity. The mean values and standard deviations (SD) of the luciferase activities from at least three independent experiments are shown.

(E) Promoter-promoter interaction at the *INTS1-MAFK* locus. The arrow boxes indicate the aligned promoter regions which were cloned in reporter gene constructs for luciferase assay.

(F) Promoter-enhancer-promoter interactions at the *C14orf102-CALM1* locus. RNA-Seq data showed that *CALM1* was highly expressed, whereas *C14orf102* only marginally transcribed (enlarged RNA-Seq track of the *C14orf102* locus).

(G) Swap assay of DNA fragments from different multigene complexes. The dotted arrow lines show the swap of elements cloned in the distal positions in the reporter gene constructs for luciferase assay.

See also Figure S5 and Table S2.

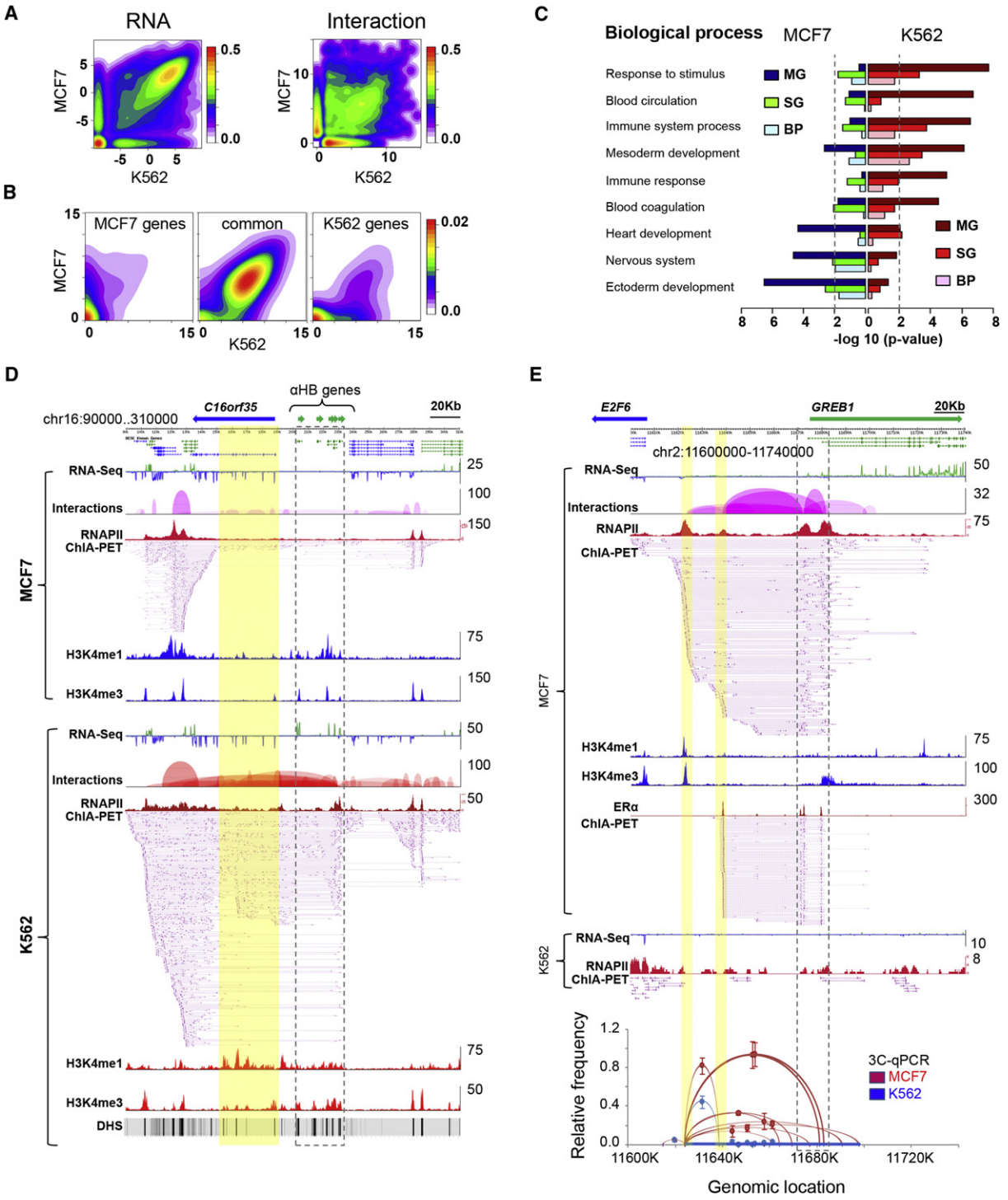

Figure 6. Cell-Specific Chromatin Interactions

(A) Contour plots of RNA-Seq data (log RPKM, left) and chromatin interactions (log PET counts, right) in MCF7 and K562 cells, showing common and cell-specific gene expression and chromatin interactions.

(B) Contour plots of interaction data (log PET counts) for genes specifically and commonly expressed in MCF7 and K562 cells.

(C) Enrichment of cell-specific GO terms in genes and chromatin interactions specific in MCF7 and K562 cells. The p value of 0.01 is marked as dotted line.

(D) An example of K562-specific chromatin interactions. α-globin genes (in dotted line box) interact with distantly located (~20 kb) DHS sites (highlighted in yellow) which are known to interact with α-globin genes. In sharp contrast, the α-globin genes in MCF7 cells are not expressed and have no interactions with the DHS sites.

bacterial operon as a mechanism for coordinated transcriptional regulation of related genes, suggesting the possibility of a chromatin-based operon mechanism (chro-operon or chroperon) for spatiotemporal regulation of gene transcription in eukaryotic nuclei. However, the ''chroperon'' expression is not dependent on the linear arrangement of the genes, but is highly dynamic and can adopt a multitude of cassette configurations because of the combinatorics permitted by the looping interactions. Alternatively, these interactions could reflect stochastic movement of proximal and distant active genes to localized transcription factories.

An important question is how these multigene complexes are organized. A likely model is that a suite of protein factors for modulating gene expression in a functional regulatory cassette may result in optimal stoichiometry when aggregated in 3D space. This clustering also draws the regulated genes into a common spatial domain, similar to how the nucleolus is organized. The interacting regions can be established and/or maintained by potential chromatin bridging proteins such as cohesins (Merkenschlager, 2010) and CTCF (Handoko et al., 2011), and this process might be facilitated by chromatin remodeling proteins (Euskirchen et al., 2011), all of which are enriched at the interacting sites defined by RNAPII ChIA-PET data.

Long-range chromatin interactions including enhancer-promoter interactions are increasingly being recognized as an important mechanism to regulate many important genes. However, methods to identify such long-range relationships have been technically challenging. High-throughput approaches such as ChIP-Seq and DNase-Seq are efficient in identifying potential regulatory sites, but lack the ability to interrogate the connectivity between the prospective enhancers and their target gene promoters. In this study using RNAPII as the protein target for ChIA-PET analysis, we identified a comprehensive repertoire of distant regulatory elements directly interacting with gene promoters. Many of them act through ultra-long-range chromatin interactions. Such distal enhancer-promoter relationships are particularly difficult to be identified by other approaches. As demonstrated in the cases of *SHH* and *IRS1*, long range interactions derived from ChIA-PET data could provide the connectivity of GWAS-identified high-risk loci to their target genes, and thus offer possible mechanistic explanations to the function of disease-associated noncoding elements. Further investigation of spatial architectures revealed in this study will enhance our understanding of transcription regulation in normal and diseased conditions of human cells.

EXPERIMENTAL PROCEDURES

Cell Culture

Five cell lines, namely MCF7 (ATCC# HTB-22), K562 (ATCC# CCL-243), HCT116 (ATCC# CCL-247), HeLa (ATCC# CCL-2.2), and NB4, were grown under standard culture conditions and harvested at log phase.

ChIA-PET

Harvested cells were cross-linked using 1% formaldehyde followed by neutralization with 0.2M glycine. Chromatin was isolated and subjected to the ChIA-PET procedure (Fullwood et al., 2009). The ChIA-PET sequence reads were analyzed using ChIA-PET Tool (Li et al., 2010). The data are available from NCBI/GEO (ID GSE33664). Control and reproducibility analyses are described in Figure S8.

RNA-Seq Data

MCF7 mRNA was isolated following the protocol described in Ruan et al. (Ruan et al., 2007) for strand-specific RNA-Seq analysis by SOLiD sequencing platform. The rest of the RNA-Seq datasets for other cell-lines were retrieved from the ENCODE data repository site (http://genome.ucsc.edu/ENCODE/).

ChIP-Seq Data

The ChIP-Seq data were retrieved from (Joseph et al., 2010), (Raha et al., 2010) and the ENCODE data repository site (http://genome.ucsc.edu/ENCODE/).

RNAPII IF Stain and DNA-FISH

MCF7 cells were fixed using 4% formaldehyde followed by permeabilization with 0.04% Triton-X. After blocking with donkey serum, cells were incubated with primary antibody (8WG16) overnight followed by Cy3 conjugated secondary antibody for 1 hr. IF-stained cells were post-fixed and subjected to dehydration by 70, 80, 100% ethanol series, rehydration with 2× SSC and denaturation in 2× SSC/50% formamide at 80°C for 40 min. Biotin-16-dUTP and digoxigenin-11-dUTP labeled DNA probes were hybridized to cells at 37°C overnight in a humid chamber. Slides were washed, stained with DAPI, mounted and visualized by a Carl Zeiss LSM confocal microscope.

Quantitative Chromosome Conformation Capture Analysis

Targeted 3C products were analyzed by qPCR. The 3C-qPCR protocol was adapted and modified from the previous publication (Fullwood et al., 2009).

Luciferase Reporter Gene Assay

Dual luciferase assays were performed as described (Pan et al., 2008). Testing fragments were cloned into pGL4.10-basic vector. Constructs were transfected into MCF7 cells, and luciferase activities were measured following standard protocols.

Statistical Analysis

All the statistical tests were executed using the R statistical package (http://www.r-project.org/).

More details are available in Extended Experimental Procedures.

SUPPLEMENTAL INFORMATION

Supplemental Information includes Extended Experimental Procedures, five tables, and eight figures and can be found with this article online at doi:10.1016/j.cell.2011.12.014.

ACKNOWLEDGMENTS

We acknowledge the Genome Technology and Biology Group at the Genome Institute of Singapore for technical support. This work was supported by Singapore A*STAR and an NIH grant (HG004456) to Y.R.

Received: July 18, 2011
Revised: October 21, 2011
Accepted: December 12, 2011
Published: January 19, 2012

(E) An example of MCF7-specific chromatin interactions around the *GREB1* locus. The far left highlighted yellow is a RNAPII interaction site that is not overlapped by ERα-bound interactions in this region. It is also the bait site for independent 3C validation of interactions in this region. Tracks included in (D) and (E) are RNA-Seq data, interaction loop view, RNAPII ChIA-PET peaks and interaction PETs, ChIP-Seq density profile of H3K4me1 and H3K4me3, and the ERα-ChIA-PET in (E). The numbers on the right of each track are the highest density value. 3C-qPCR mean values and standard error of means (SEM) from three independent experiments are shown.
See also Figure S6 and Figure S7.

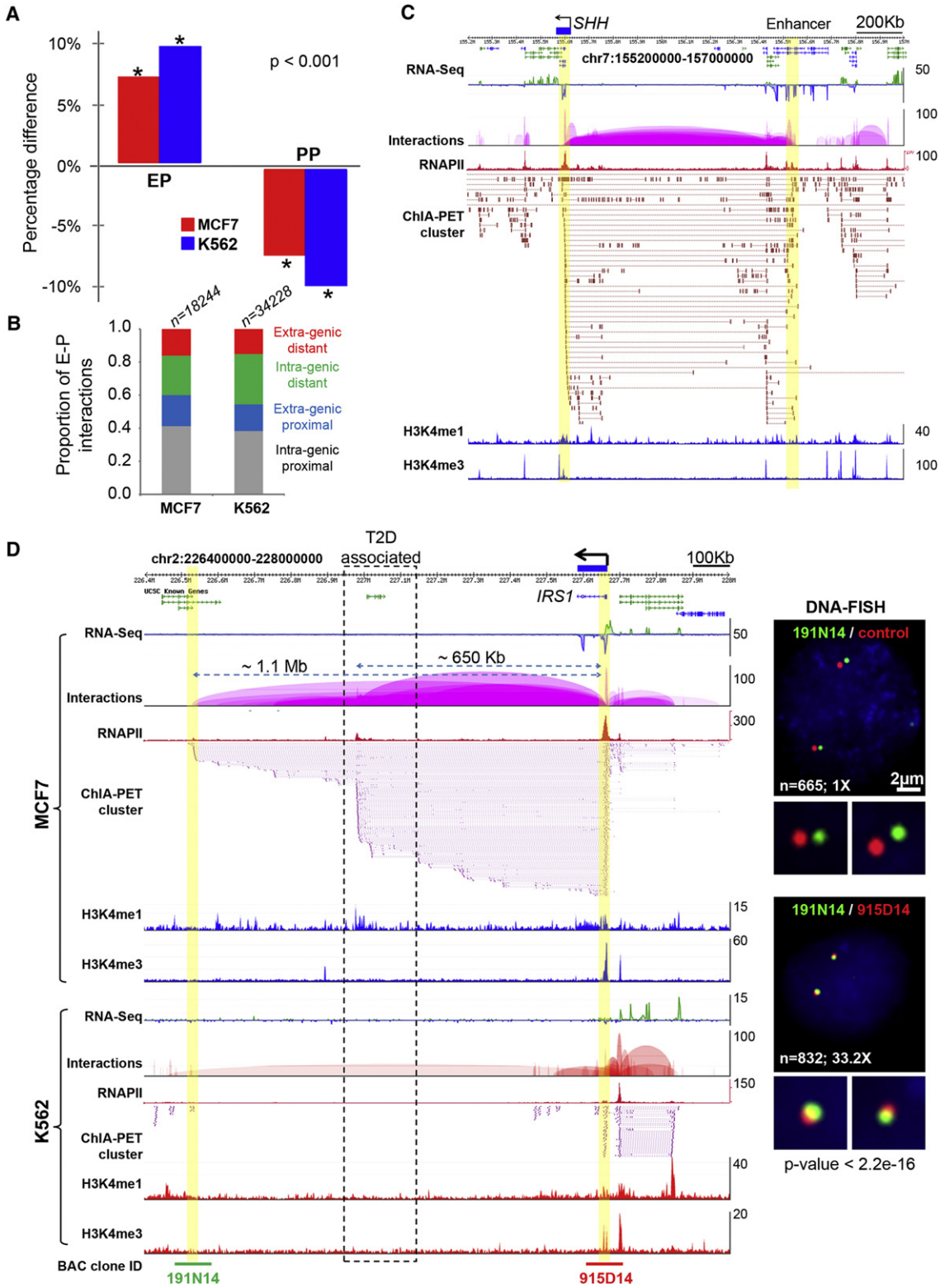

Figure 7. Long-Range Enhancers and Disease-Associated Noncoding Elements

(A) Percentage difference of enhancer-promoter (EP) and promoter-promoter (PP) interactions in cell-specific versus common genes from MCF7 and K562 cells. The representation of EP interactions is significantly increased in cell-specific interactions, while the representation of PP interactions is decreased, when compared to interactions that are common to both cell lines.

REFERENCES

Amano, T., Sagai, T., Tanabe, H., Mizushina, Y., Nakazawa, H., and Shiroishi, T. (2009). Chromosomal dynamics at the Shh locus: limb bud-specific differential regulation of competence and active transcription. Dev. Cell *16*, 47–57.

Barski, A., Cuddapah, S., Cui, K., Roh, T.Y., Schones, D.E., Wang, Z., Wei, G., Chepelev, I., and Zhao, K. (2007). High-resolution profiling of histone methylations in the human genome. Cell *129*, 823–837.

Bau, D., Sanyal, A., Lajoie, B.R., Capriotti, E., Byron, M., Lawrence, J.B., Dekker, J., and Marti-Renom, M.A. (2011). The three-dimensional folding of the alpha-globin gene domain reveals formation of chromatin globules. Nat. Struct. Mol. Biol. *18*, 107–114.

Cook, P.R. (1999). The organization of replication and transcription. Science *284*, 1790–1795.

Cope, N.F., Fraser, P., and Eskiw, C.H. (2010). The yin and yang of chromatin spatial organization. Genome Biol. *11*, 204.

Cremer, T., and Cremer, C. (2001). Chromosome territories, nuclear architecture and gene regulation in mammalian cells. Nat. Rev. Genet. *2*, 292–301.

Eisenberg, E., and Levanon, E.Y. (2003). Human housekeeping genes are compact. Trends Genet. *19*, 362–365.

Euskirchen, G.M., Auerbach, R.K., Davidov, E., Gianoulis, T.A., Zhong, G., Rozowsky, J., Bhardwaj, N., Gerstein, M.B., and Snyder, M. (2011). Diverse roles and interactions of the SWI/SNF chromatin remodeling complex revealed using global approaches. PLoS Genet. *7*, e1002008.

Fullwood, M.J., Liu, M.H., Pan, Y.F., Liu, J., Xu, H., Mohamed, Y.B., Orlov, Y.L., Velkov, S., Ho, A., Mei, P.H., et al. (2009). An oestrogen-receptor-alpha-bound human chromatin interactome. Nature *462*, 58–64.

Hah, N., Danko, C.G., Core, L., Waterfall, J.J., Siepel, A., Lis, J.T., and Kraus, W.L. (2011). A rapid, extensive, and transient transcriptional response to estrogen signaling in breast cancer cells. Cell *145*, 622–634.

Handoko, L., Xu, H., Li, G., Ngan, C.Y., Chew, E., Schnapp, M., Lee, C.W., Ye, C., Ping, J.L., Mulawadi, F., et al. (2011). CTCF-mediated functional chromatin interactome in pluripotent cells. Nat. Genet. *43*, 630–638.

Heintzman, N.D., Hon, G.C., Hawkins, R.D., Kheradpour, P., Stark, A., Harp, L.F., Ye, Z., Lee, L.K., Stuart, R.K., Ching, C.W., et al. (2009). Histone modifications at human enhancers reflect global cell-type-specific gene expression. Nature *459*, 108–112.

Hou, C., Dale, R., and Dean, A. (2010). Cell type specificity of chromatin organization mediated by CTCF and cohesin. Proc. Natl. Acad. Sci. USA *107*, 3651–3656.

Jacob, F., Perrin, D., Sanchez, C., and Monod, J. (1960). C. R. Hebd. Seances Acad. Sci. *250*, 1727–1729.

Joseph, R., Orlov, Y.L., Huss, M., Sun, W., Kong, S.L., Ukil, L., Pan, Y.F., Li, G., Lim, M., Thomsen, J.S., et al. (2010). Integrative model of genomic factors for determining binding site selection by estrogen receptor α. Mol. Syst. Biol. *6*, 456.

Kilpelainen, T.O., Zillikens, M.C., Stancakova, A., Finucane, F.M., Ried, J.S., Langenberg, C., Zhang, W., Beckmann, J.S., Luan, J., Vandenput, L., et al. (2011). Genetic variation near IRS1 associates with reduced adiposity and an impaired metabolic profile. Nat. Genet. *43*, 753–760.

Kim, T.K., Hemberg, M., Gray, J.M., Costa, A.M., Bear, D.M., Wu, J., Harmin, D.A., Laptewicz, M., Barbara-Haley, K., Kuersten, S., et al. (2010). Widespread transcription at neuronal activity-regulated enhancers. Nature *465*, 182–187.

Lettice, L.A., Horikoshi, T., Heaney, S.J., van Baren, M.J., van der Linde, H.C., Breedveld, G.J., Joosse, M., Akarsu, N., Oostra, B.A., Endo, N., et al. (2002). Disruption of a long-range cis-acting regulator for Shh causes preaxial polydactyly. Proc. Natl. Acad. Sci. USA *99*, 7548–7553.

Li, G., Fullwood, M.J., Xu, H., Mulawadi, F.H., Velkov, S., Vega, V., Ariyaratne, P.N., Mohamed, Y.B., Ooi, H.S., Tennakoon, C., et al. (2010). ChIA-PET tool for comprehensive chromatin interaction analysis with paired-end tag sequencing. Genome Biol. *11*, R22.

Merkenschlager, M. (2010). Cohesin: a global player in chromosome biology with local ties to gene regulation. Curr. Opin. Genet. Dev. *20*, 555–561.

Pan, Y.F., Wansa, K.D., Liu, M.H., Zhao, B., Hong, S.Z., Tan, P.Y., Lim, K.S., Bourque, G., Liu, E.T., and Cheung, E. (2008). Regulation of estrogen receptor-mediated long range transcription via evolutionarily conserved distal response elements. J. Biol. Chem. *283*, 32977–32988.

Pauli, D., Tonka, C.H., and Ayme-Southgate, A. (1988). An unusual split Drosophila heat shock gene expressed during embryogenesis, pupation and in testis. J. Mol. Biol. *200*, 47–53.

Raha, D., Hong, M., and Snyder, M. (2010). ChIP-Seq: a method for global identification of regulatory elements in the genome. Curr. Protoc. Mol. Biol. *Chapter 21*, Unit 21 19 21-14.

Roussel, M.J., and Lanotte, M. (2001). Maturation sensitive and resistant t(15;17) NB4 cell lines as tools for APL physiopathology: nomenclature of cells and repertory of their known genetic alterations and phenotypes. Oncogene *20*, 7287–7291.

Ruan, Y., Ooi, H.S., Choo, S.W., Chiu, K.P., Zhao, X.D., Srinivasan, K.G., Yao, F., Choo, C.Y., Liu, J., Ariyaratne, P., et al. (2007). Fusion transcripts and transcribed retrotransposed loci discovered through comprehensive transcriptome analysis using Paired-End diTags (PETs). Genome Res. *17*, 828–838.

Schoenfelder, S., Sexton, T., Chakalova, L., Cope, N.F., Horton, A., Andrews, S., Kurukuti, S., Mitchell, J.A., Umlauf, D., Dimitrova, D.S., et al. (2010). Preferential associations between co-regulated genes reveal a transcriptional interactome in erythroid cells. Nat. Genet. *42*, 53–61.

Singer, G.A., Lloyd, A.T., Huminiecki, L.B., and Wolfe, K.H. (2005). Clusters of co-expressed genes in Mamm. Genomes are conserved by natural selection. Mol. Biol. Evol. *22*, 767–775.

Su, A.I., Cooke, M.P., Ching, K.A., Hakak, Y., Walker, J.R., Wiltshire, T., Orth, A.P., Vega, R.G., Sapinoso, L.M., Moqrich, A., et al. (2002). Large-scale analysis of the human and mouse transcriptomes. Proc. Natl. Acad. Sci. USA *99*, 4465–4470.

(B) Proportional distribution of 4 classes of enhancers observed in two cell lines based on locations in relation to gene coding regions. "Intragenic proximal" enhancers locate inside of gene-body (mostly introns) and interact with the nearby promoters. "Extragenic proximal" enhancers locate outside of gene body and interact with the nearby promoters. "Intragenic distal" enhancers locate inside of gene body (mostly introns), bypass nearby genes and interact with faraway gene promoters in long-distance. "Extragenic distal" enhancers locate outside of gene body, bypass nearby genes and interact with faraway gene promoters in long-distance.

(C) Long-range interactions between *SHH* (highlighted in yellow, left) and its enhancer located about 1 Mb away in an intron of *LMBR1* (highlighted yellow, right). The *SHH* expression is specifically seen in MCF7 cells.

(D) Long-range interactions between *IRS1* promoter and two enhancers as well as strong *IRS1* expression are seen in MCF7, but not in K562 cells. The dotted line box indicates the enhancer region that contains SNPs associated with insulin resistance, type-2 diabetes (T2D) and coronary artery heart disease identified by a GWAS study. The interactions of enhancer located 1.1 Mb away to *IRS1* promoter (highlighted in yellow) is validated by DNA-FISH (right). The BAC clones and genomic segments used for DNA-FISH are indicated at the bottom.

Tracks included in (C) and (D) are RNA-Seq density profile, interaction loop view, RNAPII peaks, ChIA-PET interaction PETs, ChIP-Seq density profile of H3K4me1 and H3K4me3 marks.

See also Figure S7 and Table S5.

Taylor, J. (2005). Clues to function in gene deserts. Trends Biotechnol. *23*, 269–271.

van Steensel, B., and Dekker, J. (2010). Genomics tools for unraveling chromosome architecture. Nat. Biotechnol. *28*, 1089–1095.

Versteeg, R., van Schaik, B.D., van Batenburg, M.F., Roos, M., Monajemi, R., Caron, H., Bussemaker, H.J., and van Kampen, A.H. (2003). The human transcriptome map reveals extremes in gene density, intron length, GC content, and repeat pattern for domains of highly and weakly expressed genes. Genome Res. *13*, 1998–2004.

Visel, A., Rubin, E.M., and Pennacchio, L.A. (2009). Genomic views of distant-acting enhancers. Nature *461*, 199–205.

Zorio, D.A., Cheng, N.N., Blumenthal, T., and Spieth, J. (1994). Operons as a common form of chromosomal organization in C. elegans. Nature *372*, 270–272.

THE JOURNAL OF BIOLOGICAL CHEMISTRY VOL. 286, NO. 10, pp. 8165–8175, March 11, 2011
Printed in the U.S.A.

PIASy Inhibits Virus-induced and Interferon-stimulated Transcription through Distinct Mechanisms*[S]

Received for publication, October 17, 2010, and in revised form, December 17, 2010 Published, JBC Papers in Press, January 3, 2011, DOI 10.1074/jbc.M110.195255

Toru Kubota[‡1,2], **Mayumi Matsuoka**[§1], **Songxiao Xu**[¶], **Noriyuki Otsuki**[‡], **Makoto Takeda**[‡], **Atsushi Kato**[‡], **and Keiko Ozato**[¶]

From the Departments of [‡]*Virology III and* [§]*Bacterial Pathogenesis and Infection Control, National Institute of Infectious Diseases, Tokyo 208-0011, Japan and the* [¶]*Laboratory of Molecular Growth Regulation, Genomics of Differentiation Program, NICHD, National Institutes of Health, Bethesda, Maryland 20892-2753*

The protein inhibitor of activated STAT (PIAS) family proteins regulates innate immune responses by controlling transcription induced by Toll-like receptor, RIG-I-like receptor signaling, and JAK/STAT pathways. Here, we show that PIASy negatively regulates type I interferon (IFN) transcription. Virus infection led to enhanced type I IFN induction in PIASy null cells, and conversely PIASy overexpression reduced IFN transcription. A mutation in the LXXLL motif of the SAP domain abolished inhibition of IFN-stimulated gene expression but did not affect virus or Toll-like receptor/RIG-I-like receptor-stimulated IFN transcription, indicating that PIASy employs distinct mechanisms to inhibit virus-induced and IFN-stimulated transcription. SUMO E3 activity was not required for PIASy inhibition of IFN transcription; however, PIASy relied on the SUMO modification mechanism to inhibit IFN transcription, because the activity of the SUMO-interacting motif was required for inhibition, and knockdown of SUMO E2 enzyme UBC9 decreased inhibitory activity of PIASy. Our results demonstrate that PIASy negatively regulates both IFN transcription and IFN-stimulated gene expression through multiple mechanisms utilizing the function of different domains.

Infection of RNA viruses is recognized by two classes of pathogen recognition receptors, Toll-like receptors (TLR)[3] and RIG-I-like receptors (RLR), both of which bind viral RNAs (1–7). Once viral RNAs are recognized by these receptors, downstream signaling cascades are activated, triggering transcription of proinflammatory cytokines important for the establishment of innate and adaptive immunity (5). Among these cytokines, type I interferons (IFNs) play a major role in conferring antiviral and antimicrobial activities (8–11). TLR- and RLR-mediated production of type I IFNs and proinflammatory cytokines are regulated both positively and negatively at multiple steps of signaling cascades to minimize harmful excess inflammatory responses and to achieve fine-tuning of the effects (12–14). There is a growing list of proteins that function as a negative regulator of TLR and RLR signaling (15, 16).

PIAS (protein inhibitor of activated STAT) family proteins are encoded by four genes, *PIAS1*, *PIAS3*, *PIASx* (*PIAS2*), and *PIASy* (*PIAS4*) (17–21). The PIAS family was first discovered as an interacting partner of signal transducer and activator of transcription (STAT) (21–24). By associating with transcriptionally activated STATs, PIAS proteins negatively regulate some STAT-dependent genes (20, 21, 23–25). In addition to STATs, PIAS proteins also regulate large numbers of transcription factors involved in the broad range of gene expression that affects cell cycle regulation, immune responses, and development (18–21, 26). PIAS proteins function as a SUMO E3 ligase for a growing list of substrates, most of which are transcription factors (27–31). The conserved RING-like domain at the central portion of PIAS proteins is essential for E3 ligase activity (19–21, 32, 33). Conjugation of SUMO peptides to transcription factors alters transcriptional activity by changing conformation of substrates and creating a new surface for protein-protein interactions (26–29, 34, 35). In addition to regulating SUMO modification by its SUMO ligase activity, PIAS proteins regulate transcription through SUMO-independent mechanisms, including blocking DNA binding activity of transcription factors, recruiting transcriptional co-repressors, and translocation of transcription factors to nuclear subdomains (17–21).

Among PIAS proteins, PIAS1 and PIASy regulate the specificity and magnitude of cytokine-induced gene expression mediated by STAT1 (36, 37). In addition, PIAS1 and PIASy regulate LPS-induced cytokine production by inhibiting NFκB activity (37, 38). Thus, PIAS1 and PIASy play an important role not only in cytokine-mediated JAK/STAT pathways but also in pathogen-activated TLR/RLR pathways of cytokine production (20, 39). Prompted by these reports, we asked whether type I IFN production mediated by TLR and RLR signaling is also regulated by PIASy. We report here that PIASy inhibits virus-induced type I IFN transcription more potently than the other three PIAS members. PIASy targeted IRF3 and IRF7, transcrip-

* This work was supported, in whole or in part, by National Institutes of Health grant from the Intramural Research Program of NICHD and Trans NIH Biodefense Program. This work was also supported by Grant-in-aid 22590424 for Scientific Research (C) from the Ministry of Education, Culture, Sports, Science, and Technology of Japan.

[S] The on-line version of this article (available at http://www.jbc.org) contains supplemental Fig. 1.

[1] Both authors contributed equally to this work.
[2] To whom correspondence should be addressed. Tel.: 81-42-561-0771; Fax: 81-42-567-5631; E-mail: kubota@nih.go.jp.

[3] The abbreviations used are: TLR, Toll-like receptor; RLR, RIG-I-like receptor; RIG-I, retinoic acid-inducible gene I; IRF, interferon regulatory factor; SUMO, small ubiquitin-related modifiers; SIM, SUMO-interacting motif; IKK, IκB kinase; ISG, interferon stimulated gene; VSV, vesicular stomatitis virus; EMCV, encephalomyocarditis virus; m.o.i., multiplicity of infection; shRNA, short hairpin RNA; qRT-PCR, quantitative RT; MEF, mouse embryonic fibroblast; STAT, signal transducer and activator of transcription; ISRE, interferon-stimulated response element; TRIF, TIR domain-containing adaptor-inducing interferon β.

tion factors required for activation of the type I IFN promoter. Detailed domain analysis revealed that PIASy inhibits IRF3/IRF7-activated type I IFN transcription by a mechanism distinct from that of PIASy inhibition of IFN-stimulated gene (ISG) induction by STAT1. Additionally, we show that PIASy relies on the SUMO conjugation mechanism through the SUMO-interacting motif (SIM) to inhibit type I IFN transcription, but without relying on its own E3 ligase activity. Together, our findings highlight the diversity and complexity of PIASy-mediated negative regulation of IFN and IFN-stimulated transcription, thus influencing innate immunity.

EXPERIMENTAL PROCEDURES

Cells Culture—Mouse embryonic fibroblasts (MEFs) from PIASy$^{+/+}$ and PIASy$^{-/-}$ mice were grown in Dulbecco's modified Eagle's medium (DMEM)/high glucose supplemented with 10% FCS and antibiotics (Invitrogen). Human embryonic kidney (HEK) 293T cells were grown in DMEM containing 10% fetal bovine serum.

Plasmids and Reagents—cDNA fragments of murine PIAS1, PIAS3, PIASxa, PIASxb, and PIASy were generated from total RNA of NIH3T3 cells by the standard RT-PCR technique and were inserted into pcDNA3.1/HA and pMSCV/HA retroviral vector. To construct mutants for PIASy, appropriate substitutions were introduced into the pcDNA3.1-PIASy-HA and pMSCV-PIASy-HA using the QuickChange site-directed mutagenesis kit (Stratagene, La Jolla, CA). T7-SUMO1/GA was generated from the T7-SUMO1 expression plasmid (40). Murine IRF3 and IRF7 constructs were described previously (40). Human VISA cDNA was amplified from total RNA of HEK293T cells and inserted into pcDNA-2×Myc and pcDNA-V5 vector. Myc-TRIF, FLAG-IKKϵ, FLAG-TBK1, and IFNα1 promoter-luciferase reporter plasmids were gifts from Dr. Rongtuan Lin (McGill University, Montreal, Canada). 2×FLAG-RIG-IN (constitutively active RIG-I) and IFNβ promoter-luciferase reporter plasmids were gifts from Dr. Takashi Fujita (University of Kyoto, Kyoto, Japan). For constructing shRNA retroviral vector for human UBC9, an oligonucleotide fragment (target sequence: 5′-aacagatcctattaggaatac-3′) was inserted into pSUPER.retro (Oligoengine, Seattle). Retroviral preparations were made according to the manufacturer's instructions. As a control, a retroviral vector with a scrambled oligonucleotide fragment was prepared and tested in parallel. Mouse monoclonal antibodies against FLAG M2 and α-tubulin were purchased from Sigma. Rabbit and mouse antibodies for the T7 tag were purchased from Abcam (Cambridge, MA) and Novagen (Gibbstown, NJ), respectively. Rabbit antibody against murine IRF3 was from Zymed Laboratories Inc.. Rabbit antibodies against phospho-IRF3 (Ser(P)-396) and phospho-IRF3 (Ser(P)-386) were from Cell Signaling Technology (Danvers, MA) and EPITOMICS (Burlingame, CA), respectively. Rat antibody against HA was from Roche Diagnostics. Mouse monoclonal antibody against UBC9 was from Transduction Laboratories (Lexington, KY), and goat antibodies against rabbit IgG Alexa Fluor 488 and mouse IgG Alexa Fluor 546 were from Invitrogen. Recombinant human IFNβ was from Toray Industries, Inc. (Tokyo, Japan).

GFP-Sendai Virus Infection—Recombinant Sendai virus expressing GFP was generated and titrated as described elsewhere (41, 42). GFP signals in Sendai virus-infected cells were monitored by Axiovert 200 fluorescent microscope (Carl Zeiss Japan, Tokyo, Japan).

Quantitative (q) RT-PCR—PIASy$^{+/+}$ and PIASy$^{-/-}$ MEFs with or without murine PIASy (1×10^6) were infected with vesicular stomatitis virus (VSV) or EMCV for the indicated time period at an m.o.i. of 5. Total RNA prepared using TRIzol reagent (Invitrogen) was reverse-transcribed with the Transcriptor First Strand cDNA synthesis kit (Roche Diagnostics). The amounts of IFNβ, IFNα4, and hypoxanthine-guanine phosphoribosyltransferase cDNA were measured by using Universal ProbeLibrary and LightCycler 480 (Roche Diagnostics) according to the manufacture's instructions. Primers for qRT-PCR were designed by the Probe Finder software (Roche Diagnostics).

Luciferase Reporter Assay—HEK293T cells were plated in 24-well plates at 3×10^4/0.5 ml and transiently transfected with the indicated combinations of plasmids using Lipofectamine 2000 (Invitrogen) according to the manufacturer's recommendations. Eighteen h post-transfection, cells were lysed, and luciferase activity was measured by using the Dual-Luciferase reporter assay kit (Promega) according to the manufacturer's procedure. Alternatively, cells were treated with 10^3 units/ml IFNβ for 6 h starting at 18 h post-transfection. *Renilla* luciferase activity was used for normalization.

Immunoblot Analysis—Whole cell extracts were prepared using lysis buffer containing 150 mM NaCl, 50 mM Tris-HCl, pH 7.5, 4 mM EDTA, 0.1% sodium deoxycholate, 1% Nonidet P-40, 0.1% SDS, complete protease inhibitor mixture (Roche Diagnostics). For Phos-tag PAGE, cells were lysed using lysis buffer without EDTA. Extracts were separated by SDS-PAGE with or without Phos-tag AAL-107 (NARD Institute, Hyogo, Japan) and immunoblotted as described previously (40).

Immunoprecipitation—293T cells (3×10^6) were transfected with a total of 3.3 μg of plasmid DNA using Lipofectamine 2000 (Invitrogen). Twelve h later, cells were lysed using lysis buffer containing 20 mM *N*-ethylmaleimide (Sigma). Lysates were centrifuged, and supernatants were incubated with anti-T7-agarose overnight with gentle rotation at 4 °C. Immune complexes were washed four times with *N*-ethylmaleimide containing lysis buffer, separated on SDS-PAGE, and subjected to immunoblot analysis.

Detection of SUMO-conjugated Proteins—To detect SUMO-conjugated proteins, 293T cells were transfected with the indicated plasmids, and extracts were prepared as above. Extracts were separated by SDS-PAGE and analyzed by immunoblot using the indicated antibodies.

Immunofluorescence Analysis—MEFs retrovirally transduced with or without murine PIASy-HA were plated on coverslips and incubated for 24 h. Cells were then infected with Sendai virus at an m.o.i. of 5 for 8 h and fixed with 3.7% paraformaldehyde. After two washes, cells were permeabilized with 0.2% Triton X-100 for 5 min and incubated at 4 °C with a blocking solution (PBS containing 3% BSA) for 30 min. The primary antibodies were added into the blocking solution at a 1:500 dilution, and cells were incubated for 4 h at 4 °C. After three

washes, cells were then incubated with secondary antibodies for 4 h at 4 °C and counterstained with Hoechst for 1 min. Stained cells were viewed on a BZ8000 fluorescence microscope (Keyence, Osaka, Japan).

RESULTS

PIASy Negatively Regulates Virus-induced Type I IFN Expression—To investigate whether PIASy is involved in the regulation of virus-induced type I IFN production, PIASy$^{-/-}$ and PIASy$^{+/+}$ MEFs were infected by VSV or EMCV. Infection by these viruses is recognized by RIG-I and MDA-5, respectively (2, 5). The amount of IFNβ and IFNα4 mRNA was measured at various time points during 24 h of infection by quantitative real time-reverse transcription PCR (qRT-PCR). As shown in Fig. 1*A*, levels of both IFNβ and IFNα4 mRNA were markedly higher in PIASy$^{-/-}$ MEFs than in PIASy$^{+/+}$ MEFs at all time points tested. Similar increased production of type I IFN mRNA was observed after EMCV infection (Fig. 1*B*), indicating that PIASy inhibits both RIG-I- and MDA-5-driven type I IFN induction. We next tested whether increased induction of type I IFNs by PIASy deficiency can be reversed by ectopic expression of PIASy. HA-tagged PIASy was retrovirally transduced into PIASy$^{+/+}$ and PIASy$^{-/-}$ MEFs, and VSV-induced type I IFN production was measured (Fig. 1*C*). Overexpression of PIASy decreased VSV-induced type I IFN production in both PIASy$^{+/+}$ and PIASy$^{-/-}$ cells. Thus, PIASy acted as a negative regulator of type I IFN induction for both "loss of function" and "gain of function" experiments. We next tested whether loss of PIASy affected virus growth (Fig. 1*D*). PIASy$^{+/+}$ and PIASy$^{-/-}$ MEFs were infected with GFP-Sendai virus at various m.o.i. values, and viral growth was monitored by GFP fluorescent signals. GFP signals in PIASy$^{+/+}$ cells were clearly much greater than in PIASy$^{-/-}$ cells at 12 h post-infection with m.o.i. of 2.5, 0.5, and 0.1, although a difference was not clear with an m.o.i. of 0.02. Similarly, GFP signals were much higher in PIASy$^{+/+}$ cells than PIASy$^{-/-}$ cells at 24 and 36 h post-infection (Fig. 1*E*). These results indicate that PIASy$^{-/-}$ cells are more resistant to Sendai virus infection, presumably due to greater production of type I IFNs.

PIASy Inhibits Type I IFN Promoter Activity Stimulated by the Activated Form of IRF3 and IRF7—Recognition of viral RNA by RIG-I leads to the activation of downstream signaling molecules such as VISA, TBK1, IKKϵ, IRF3, and IRF7 (5, 6, 43, 44). We next sought to determine a step within the signaling cascade that PIASy targets. As shown in Fig. 2*A*, IFNβ promoter activity was activated by transfection of an active form of RIG-I (RIG-IN), VISA, TBK1, IKKϵ, and activated forms of IRF3 and IRF7 (IRF3/5D and IRF7/6D, respectively). In all cases, co-expression of PIASy decreased IFNβ promoter activity in a dose-dependent manner. These results suggested that PIASy inhibited a step downstream from IRF3 and IRF7 phosphorylation. If so, phosphorylation of IRF3 and IRF7 and their subsequent nuclear translocation would not have been affected by PIASy overexpression. To test this possibility, 293T cells were transfected with Myc-tagged VISA, and FLAG-tagged IRF3 along with PIASy and phosphorylation of IRF3 were detected by Phos-tag PAGE. As shown in Fig. 2*B*, slow migrating phosphor-IRF3 bands were detected in Myc-VISA-expressed cells in the presence and absence of PIASy expression (*lanes 6–8 versus 2–4*). We also tested VISA-induced phosphorylation of IRF3 by using anti-phospho-IRF3 antibodies. Co-expression of VISA increased phosphorylation of IRF3 at Ser-396 and Ser-386 and was not affected by PIASy (Fig. 2*C*). Similar results were observed when IRF3 phosphorylation was induced by TRIF (data not shown). We next tested whether PIASy affects virus-induced nuclear translocation of IRF3. Cells transfected with HA-tagged PIASy or empty vector were infected with Sendai virus and stained with anti-HA and anti-IRF3 antibodies at 8 h post-infection (Fig. 2*D*). As expected, PIASy localized to the nucleus before and after virus infection (45). After infection, IRF3 translocated to the nucleus irrespective of PIASy transfection. These results indicate that PIASy inhibits type I IFN promoter activation without interfering with phosphorylation and nuclear translocation of IRF3.

We next tested whether PIASy inhibits IFN promoter activity that was also activated by TRIF. As shown in Fig. 2*E*, TRIF and VISA overexpression increased IFNβ and IFNα1 promoter activity, which was inhibited by co-expression of PIASy. In addition, PIASy inhibited TRIF- and VISA-induced activation of ISRE promoter activity, again in a dose-dependent manner. These results indicate that PIASy negatively regulates TLR- and RLR-induced IFN transcription as well as ISRE promoter activity. We tested whether other PIAS proteins also regulate TLR/RLR-mediated type I IFN promoter activity and found that other PIAS proteins, except PIASy, do not significantly inhibit IFNβ promoter activity, although modest inhibition was detected by the highest dose of PIAS1 in TRIF-induced promoter activity (supplemental Fig. S1).

LXXLL Motif in the SAP Domain Is Not Involved in the Inhibition of Type I IFN Transcription—PIASy has been reported to inhibit IFNγ-mediated activation of IFN stimulated genes (ISGs) by preventing STAT1-dependent activation of ISRE promoter activity (37, 45). Although type I IFN transcription is initially activated by IRF3/7, it is further enhanced by the subsequent IFN-positive feedback loop activated by STAT1 and the ISGF3 complex (46–48). Thus, it was possible that inhibition of type I IFN promoter activity was due to PIASy inhibition of STAT1 activity. It was reported that the conserved L*XX*LL motif in the N-terminal SAP domain of PIASy critically contributes to the inhibition of STAT1-dependent transcription (45). We generated a mutant PIASy in which all three leucine residues in the L*XX*LL motif were substituted to alanine (referred to *PIASy/mSAP*, Fig. 3*A*), which was retrovirally introduced to PIASy$^{-/-}$ cells. The effect of these mutations was first tested on IFNβ-mediated ISG transcription. As shown in Fig. 3*B*, mRNA levels of three ISGs, ISG15, IFI56, and IRF7, were reduced upon wild type (WT) PIASy expression. In contrast, ISG mRNA levels were comparable in PIASy/mSAP-expressing cells and control cells. The protein levels of WT and PIASy/mSAP were also comparable in these cells (Fig. 3*C*). We also tested the effect of WT and PIASy/mSAP on IFNβ-stimulated ISRE promoter activity and found that PIASy/mSAP did not inhibit ISRE promoter activity, although WT PIASy did (Fig. 3*D*). These results indicate that the L*XX*LL motif is required for the inhibition of IFN-dependent ISG expression. We next investigated whether the PIASy/mSAP also fails to inhibit

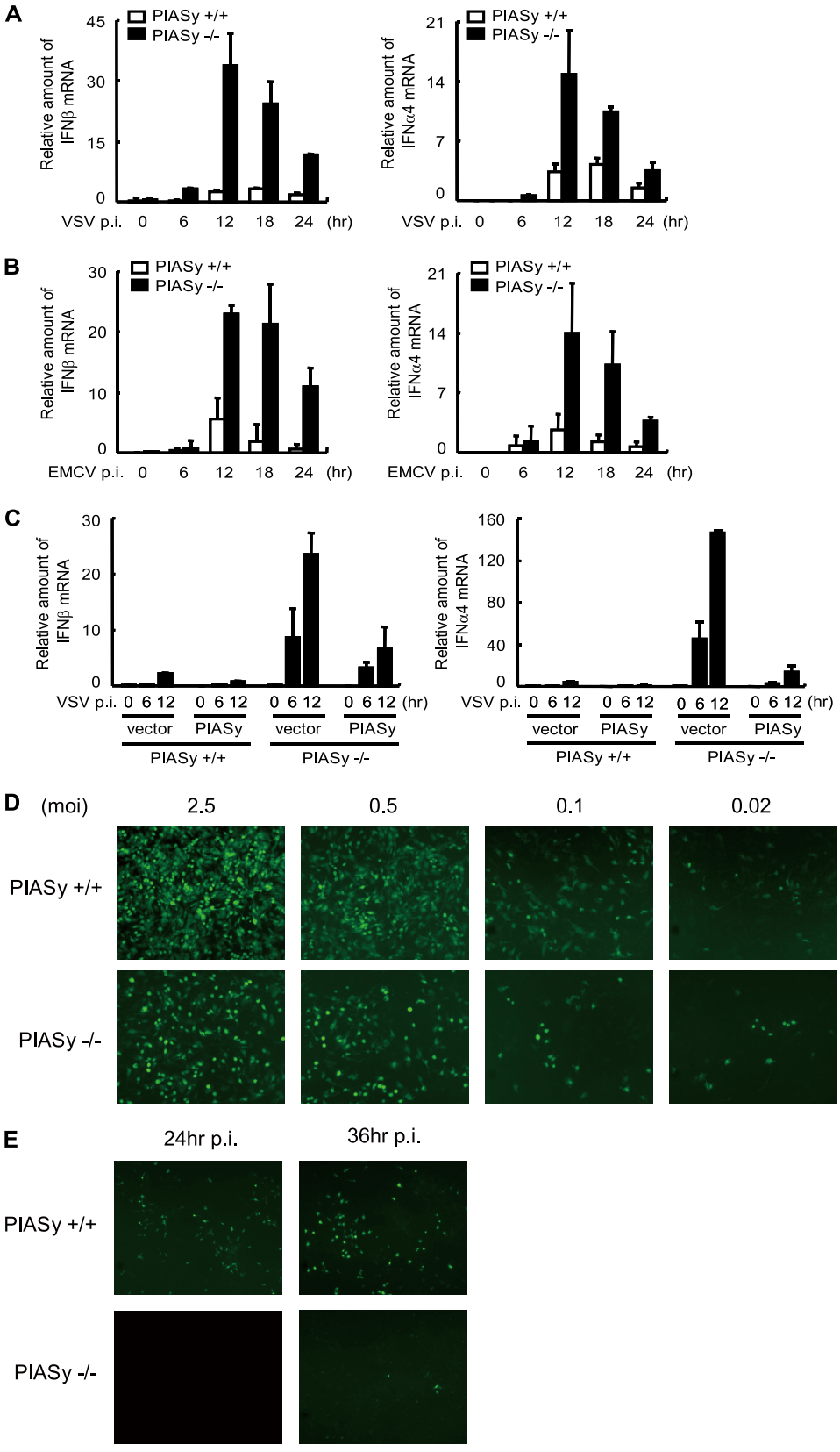

FIGURE 1. **PIASy inhibits virus-induced activation of type I IFN promoters.** *A* and *B*, PIASy$^{+/+}$ and PIASy$^{-/-}$ MEFs were infected with VSV (*A*) or EMCV (*B*). IFNβ (*left panel*) and IFNα4 (*right panel*) mRNA at indicated time post-infection (*p.i.*) were measured by qRT-PCR, and data were normalized by hypoxanthine-guanine phosphoribosyltransferase mRNA. The values represent the average of three samples ± S.D. *C*, PIASy$^{+/+}$ and PIASy$^{-/-}$ MEFs expressing PIASy or empty vector were infected with VSV, and IFNβ (*left panel*) and IFNα4 (*right panel*) mRNA at the indicated time post-infection (*p.i.*) were quantified as in *A*. *D* and *E*, PIASy$^{+/+}$ and PIASy$^{-/-}$ MEFs were infected with GFP-Sendai virus at the indicated m.o.i. for 12 h (*D*) or at an m.o.i. of 0.02 for the indicated time post-infection (*p.i.*) (*E*). GFP signals were detected by microscopic inspection.

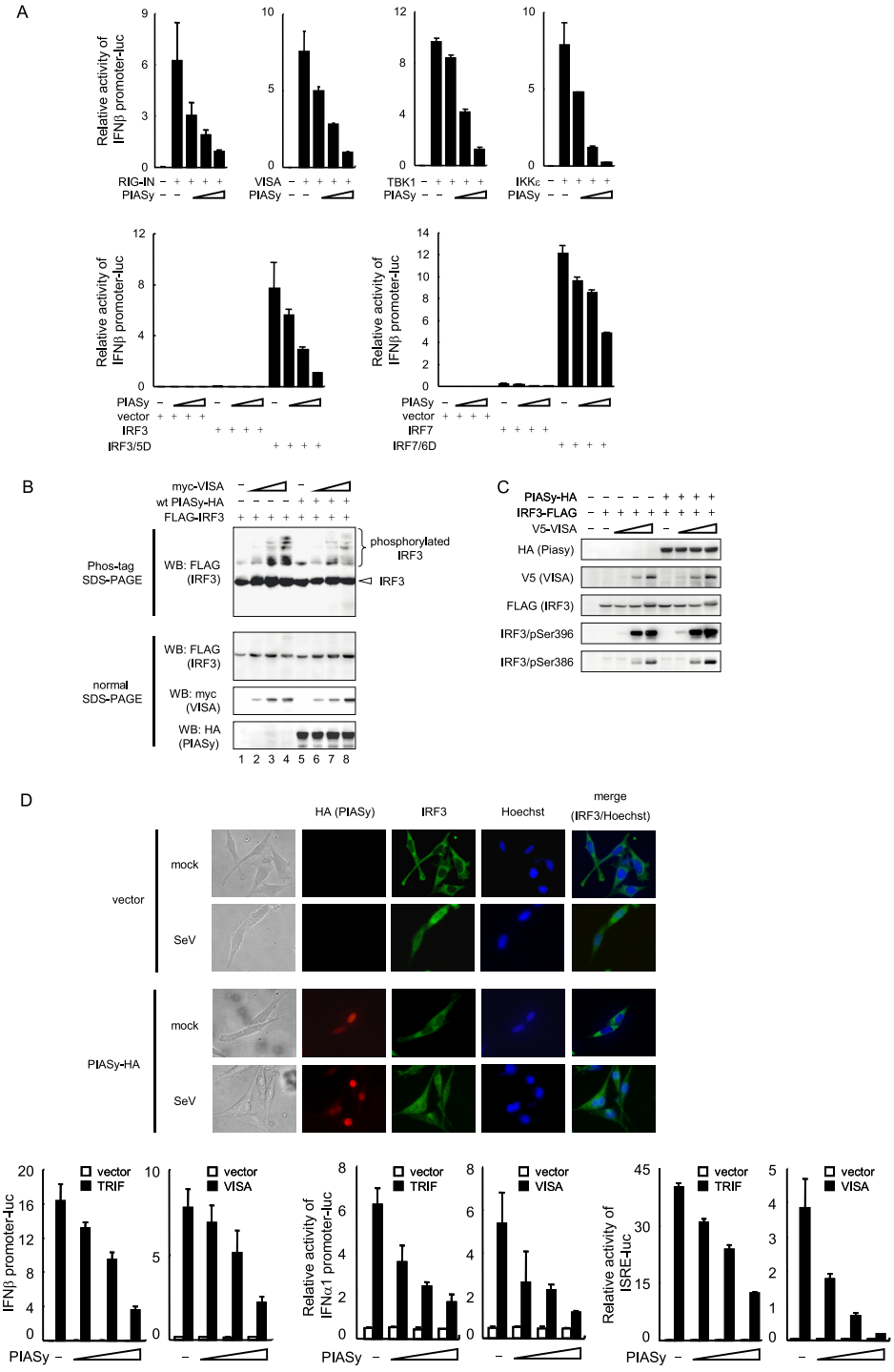

FIGURE 2. **PIASy inhibits transcriptional activity of phosphorylated IRF3.** *A,* 293T cells were transfected with indicated activators of IFNβ promoter, IFNβ promoter-luciferase reporter, and increasing doses of PIASy for 18 h. The luciferase activities were quantified by normalizing with *Renilla* luciferase activities. *B* and *C,* 293T cells were transfected with IRF3-FLAG, with or without PIASy-HA, and increasing doses of Myc-VISA (*B*) or V5-VISA (*C*) for 24 h. Whole cell extracts were tested in the Phos-tag SDS-PAGE (*B, top panels*) or standard normal SDS-PAGE (*B, lower panels* and *C*) by Western blot (*WB*) with the indicated antibodies. *D,* MEFs retrovirally transduced by empty vector or PIASy-HA were infected with Sendai virus (*SeV*) for 8 h. Fixed cells were stained with anti-HA, and anti-IRF3 antibodies and were viewed by the fluorescent microscope. *E,* 293T cells were transfected with indicated promoter-luciferase reporter with or without TRIF or VISA and increasing amounts of PIASy for 18 h. Promoter activities were quantified as in *A*.

virus-induced type I IFN induction. As shown in Fig. 3*E*, mRNA levels of IFNβ and IFNα4 were reduced in PIASy/mSAP-expressing cells to a degree similar to that in WT PIASy-expressing cells. Consistent with these data, activation of IFNβ promoter activity by VISA and TRIF was similarly inhibited by PIASy/mSAP and WT PIASy but not by PIAS3 (Fig. 3*F*). Thus, the L*XX*LL motif is dispensable for the inhibition of type I IFN induction by PIASy. These results indicate that PIASy inhibits type I IFN transcription by a mechanism distinct from that by which PIASy inhibits STAT1-mediated ISG induction. Supporting this idea, virus-induced ISG15, ifi56, and IRF7 mRNA levels were reduced by PIASy/mSAP as well as by WT PIASy, in

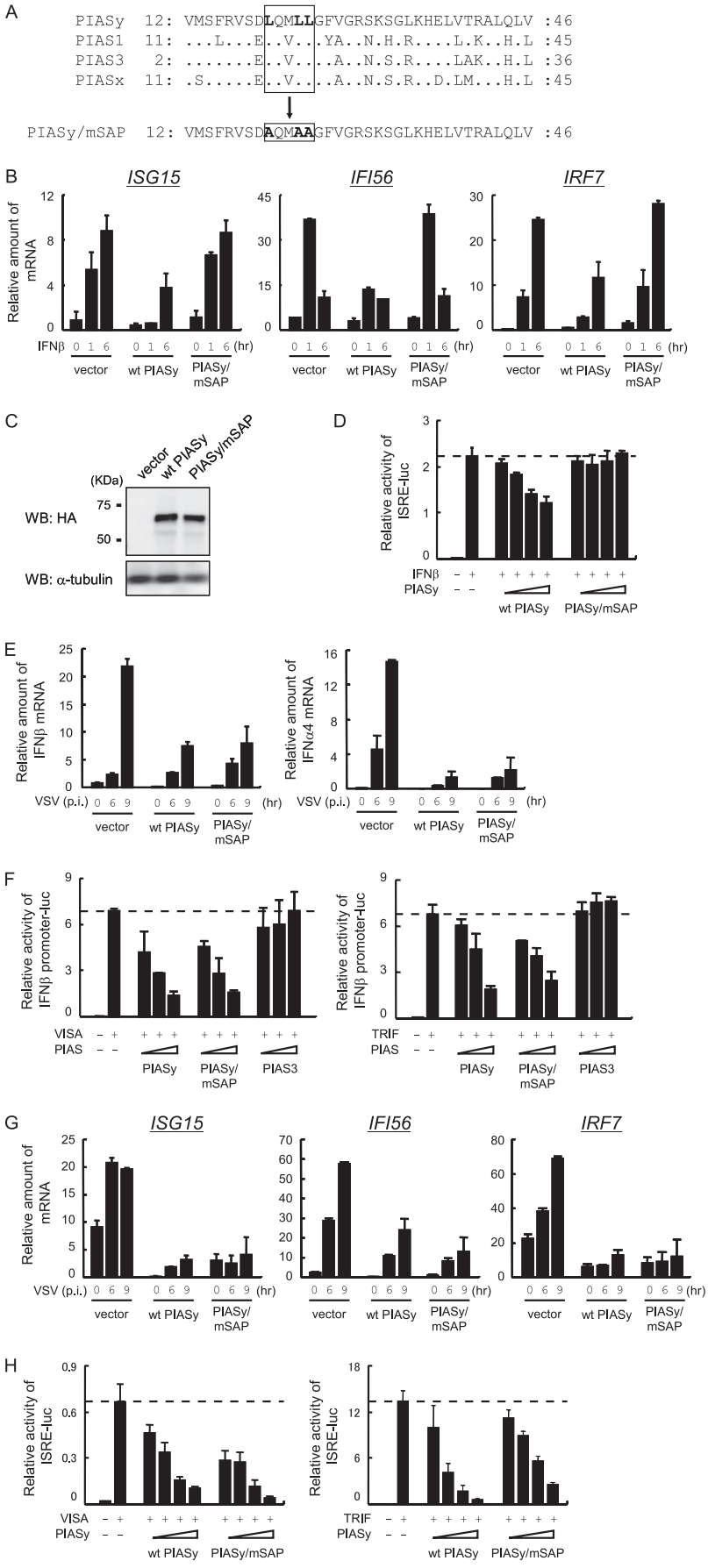

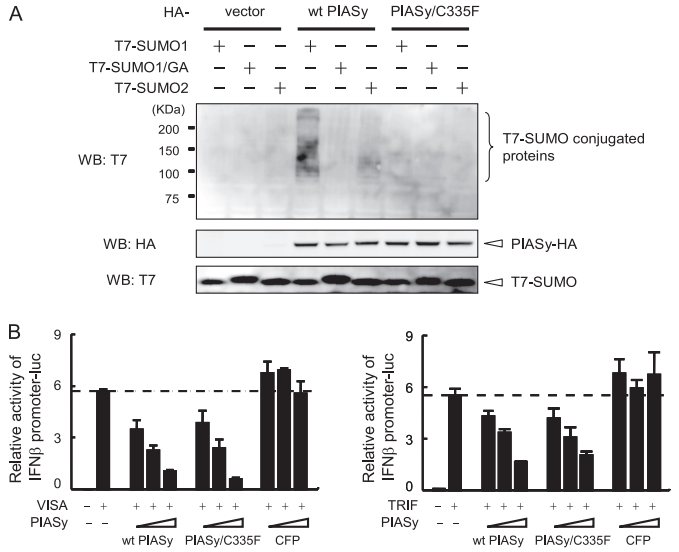

FIGURE 4. **SUMO E3 activity is not required for inhibition of TLR and RLR signaling by PIASy.** *A,* HA-tagged WT PIASy or PIASy/C335F was transfected to 293T cells together with T7-tagged WT SUMO1, SUMO1/GA, or SUMO2. Whole cell extracts were subjected to Western blot (*WB*) analysis with the indicated antibodies. *B,* 293T cells were transfected with VISA (*left*) or TRIF (*right*), IFNβ promoter reporter, and increasing amounts of WT PIASy, PIASy/C335F, or cyan fluorescent protein (*CFP*). Luciferase activities were quantified by normalizing with *Renilla* luciferase activities.

contrast to those induced by IFNβ (Fig. 3*G*). In addition, both WT PIASy and PIASy/mSAP inhibited VISA- or TRIF-induced ISRE activity in a dose-dependent manner (Fig. 3*H*). These results lead us to conclude that the L*XX*LL motif is required for inhibition of STAT1-mediated ISG transcription but not for inhibition of IRF3- and IRF7-mediated IFN transcription.

SUMO E3 Activity of PIASy Is Not Required for the Inhibition of Type I IFN Transcription—To study whether SUMO E3 ligase activity of PIASy is required for the inhibition of type I IFN transcription, we constructed a mutant PIASy in which the third cysteine residue of the RING-like domain was substituted by phenylalanine (PIASy/C335F). WT PIASy and PIASy/C335F were expressed in 293T cells together with T7-tagged SUMO1, SUMO1/GA, a conjugation-defective mutant (26), or SUMO2. Immunoblot data in Fig. 4*A* showed that WT PIASy, but not PIASy/C335F, produced slow migrating SUMO1- or SUMO2-conjugated proteins. These bands were not generated when T7-SUMO1 was replaced by T7-SUMO1/GA, as expected. Thus, PIASy/C335F no longer has a SUMO ligase activity. We next tested whether PIASy/C335F inhibits VISA- and TRIF-mediated type I IFN transcription. As shown in Fig. 4*B*, VISA- and TRIF-induced IFNβ promoter activity was inhibited by PIASy/C335F to a similar degree as WT PIASy in a dose-dependent manner. Cyan fluorescent protein expression tested as a negative control did not inhibit IFNβ promoter activity. These results indicate that PIASy inhibits VISA- and TRIF-induced type I IFN induction independent of its SUMO E3 ligase activity.

C-terminal SUMO-interacting Motif of PIASy Is Involved in the Inhibition of Type I IFN Transcription—We tested all four PIAS members for their ability to inhibit type I IFN transcription. As shown in supplemental Fig. S1, only PIASy had significant inhibitory activity. Among the PIAS proteins, the C-terminal region after the central RING-like domain is variable, and PIASy differs most from other members in this region (Fig. 5*A*). Thus we considered it possible that the C-terminal portion of PIASy is responsible for its inhibitory activity. To test this possibility, a series of C-terminal deletion mutants were generated and tested for VISA- or TRIF-induced IFNβ promoter activity. As shown in Fig. 5, *A* and *B*, transfection of the smallest deletion, PIASy/1–489 led to inhibition of IFNβ promoter activity in a manner similar to full-length PIASy. However, no inhibition was observed when the deletion was extended further, indicating that the region around amino acid 474 is critical for the inhibition of IFNβ promoter activity. This region contains a cluster of acidic amino acids (Fig. 5*C*). Although the functional significance of the acidic cluster has yet to be fully studied, a report suggested that serine residues juxtaposed to the acidic cluster are a potential phosphorylation site of CK2 protein kinase required for activity of the SUMO-interacting motif (SIM) (49). We therefore investigated the ability of these C-terminal deletion mutants to interact with SUMO peptides in a noncovalent manner. In Fig. 5*D*, HA-tagged WT PIASy and deletion mutants were transfected along with T7-tagged SUMO1/GA, and lysates were immunoprecipitated with anti-T7 antibody. Whereas full-length PIASy and PIASy/1–489 co-precipitated SUMO1/GA, all other mutants did not, verifying that the acidic cluster is required for noncovalent association of PIASy with SUMO. Given that SUMO binding activity and the IFNβ promoter inhibitory activity correlated well, we next tested whether noncovalent association of PIASy with SUMO peptides is important for inhibition of type I IFN production. To this end, two mutants were generated; first, hydrophobic amino acids in the SIM core were substituted to alanine, and second, potential target serine residues of CK2 were substituted to alanine (Fig. 5*C*, *V463/464A* and *S472–474A*, respectively). These mutants were introduced into PIASy$^{-/-}$ MEF cells and tested for possible inhibition of VSV-induced type I IFN mRNA expression. As shown in Fig. 5*E*, WT PIASy and S472/474A strongly inhibited type I IFN mRNA expression, although V463/464A caused noticeably less inhibition both in IFNβ and IFNα4 mRNA expression. Expression levels of transfected PIASy were similar and did not change during virus infection (Fig. 5*F*). The activity of these mutants

FIGURE 3. **L*XX*LL motif is not involved in the regulation of IRF3- and IRF7-mediated promoter activity.** *A,* alignment of SAP domain of murine PIAS proteins. Conserved L*XX*LL motif and PIASy/mSAP mutation are *boxed*. *B,* PIASy$^{-/-}$ MEF were transfected with WT PIASy or PIASy/mSAP. IFNβ was treated for indicated times, and mRNA for ISG15, IFI56, and IRF7 were quantified by qRT-PCR and by normalizing with hypoxanthine-guanine phosphoribosyltransferase mRNA. *C,* whole cell extracts in *B* were Western blotted (*WB*) with the indicated antibodies. *D,* 293T cells were transfected with ISRE reporter and increasing doses of WT PIASy or PIASy/mSAP. Cells were treated with IFNβ for 6 h, and luciferase activities were quantified by normalizing with *Renilla* luciferase activities. *E,* cells in *B* were infected with VSV for the indicated times, and IFNβ (*left panel*) and IFNα4 (*right panel*) mRNAs were quantified. *F,* 293T cells were transfected with VISA (*left panel*) or TRIF (*right panel*), IFNβ promoter reporter, and increasing amount of WT PIASy, PIASy/mSAP, or PIAS3. Luciferase activities were quantified as in *D*. *G,* cells in *B* were infected with VSV for the indicated times, and mRNAs were quantified as in *B*. *H,* 293T cells were transfected with VISA (*left panel*) or TRIF (*right panel*), ISRE reporter, and increasing doses of WT PIASy or PIAS/mSAP. Luciferase activities were quantified as in *D*.

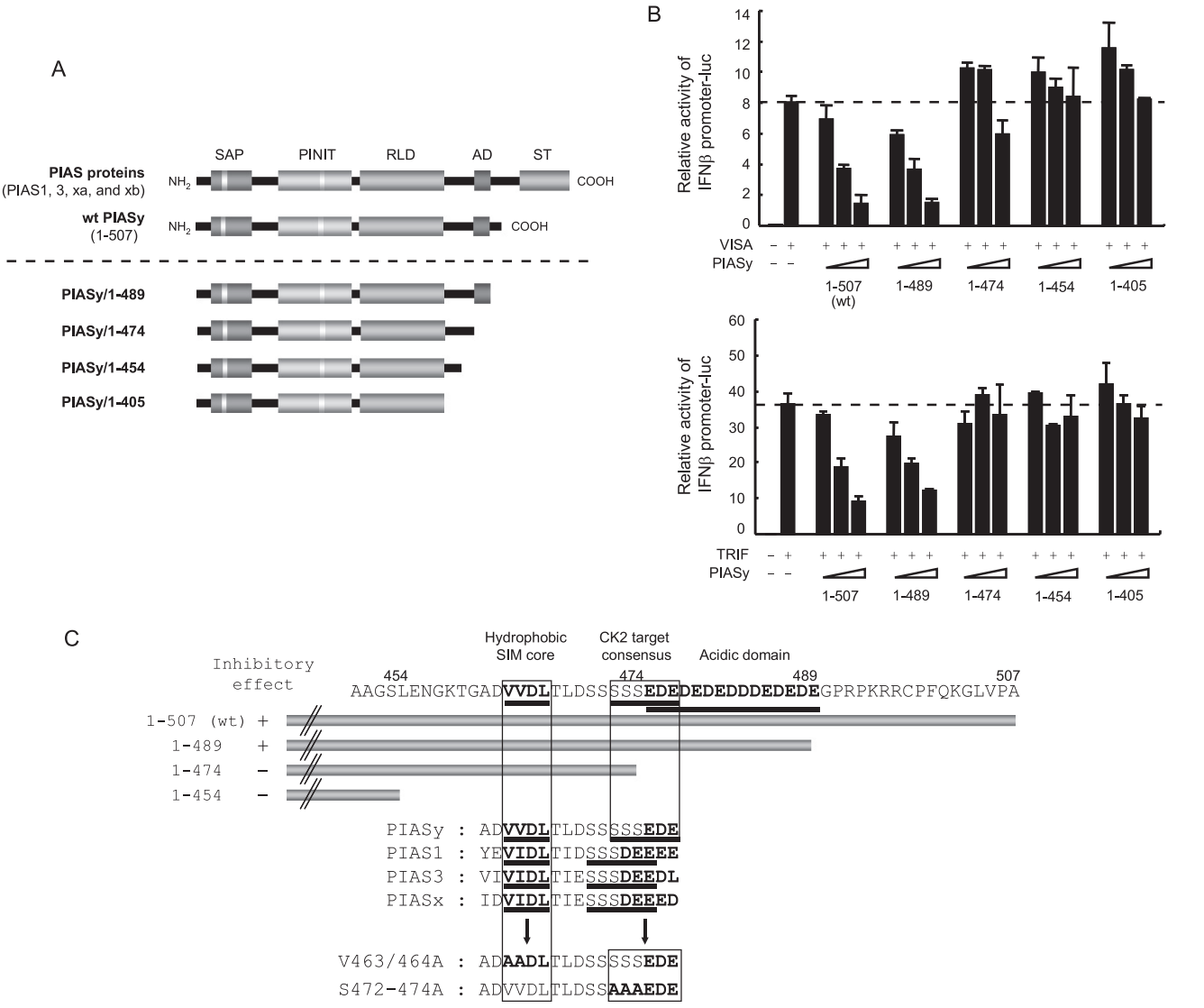

was further examined in an IFNβ reporter assay (Fig. 5*G*). WT PIASy and S472/474A repressed VISA- and TRIF-induced IFN promoter activity in a dose-dependent manner. However, V463/464A did not appreciably inhibit IFNβ promoter activity. These results indicate that the core hydrophobic residues in the putative SIM, but not the serine residues juxtaposed to the acidic cluster, are required for PIASy inhibition of type I IFN transcription.

SUMO Conjugation Mechanism Is Required for PIASy Inhibition of Type I IFN Transcription—Given that hydrophobic residues in the PIASy SIM are critical for inhibition of type I IFN induction, we next investigated whether the SUMO modification mechanism is involved in the PIASy inhibition of IFN transcription. To this end, we constructed an shRNA vector for UBC9, the sole E2 enzyme of the SUMO conjugation cascades. Data in Fig. 6*A* show that this vector stably knocked down UBC9 protein expression of IFNβ reporter activity by the activated forms of IRF3 and IRF7 (Figs. 5*D* and 6*D*, respectively) and was slightly higher in UBC9 knockdown (KD) cells than that in control shRNA-expressing cells (Fig. 6*B*). We then tested IFNβ reporter activity in UBC9 KD cells expressing PIASy. As shown in Fig. 6*C*, in UBC9 KD cells, IFNβ reporter activities stimulated by both IRF3/5D and IRF7/6D were higher than in control cells at all doses of PIASy tested. These results indicate that SUMO conjugating activity is required for the inhibition of type I IFN production by PIASy. Thus, it is likely that PIASy inhibits type I IFN promoter activity by interacting with a SUMOylated factor through the SIM. We previously showed that SUMO is covalently conjugated to IRF3 mainly through Lys-152 (40). We asked whether SUMOylated IRF3 is a main factor that binds to PIASy SIM, leading to PIASy-mediated inhibition of type I IFN induction. In Fig. 6*D*, IRF3/5D and the SUMOylation-defective mutant IRF3/5D/K152R were co-transfected with PIASy, and IFNβ promoter activity was measured. PIASy inhibited both IRF3/5D- and IRF3/5D/K152R-induced promoter activity, whereas the SIM mutant, V463/464A did not. These results indicate that IRF3 is not a major factor required for binding to SIM to confer inhibitory activity upon PIASy.

DISCUSSION

In this study, we investigated the contribution of PIASy to the regulation of type I IFN transcription. We show that VSV and EMCV infection results in greater type I IFN induction in PIASy$^{-/-}$ cells than PIASy$^{+/+}$ cells, although ectopic expression of PIASy led to reduced IFN expression. Accordingly, PIASy$^{-/-}$ cells exhibited greater antiviral activity against Sendai virus. PIASy inhibited both TRIF- and VISA-induced activation of type I IFN promoter activities, indicating that it affects both TLR- and RLR-mediated type I IFN gene activation. It is likely that PIASy does not act on an early step of TLR/RLR signaling cascades but rather acts on a step after IRF3 and IRF7 are phosphorylated and translocated into the nucleus, considering that PIASy predominantly localizes to the nucleus and PIASy efficiently inhibited type I IFN promoter activity by the activated forms of IRF3 and IRF7. Supporting this view, ectopic PIASy expression did not change VISA- and TRIF-stimulated IRF3 phosphorylation. Given that PIASy is capable of interacting with IRF3 and IRF7, it likely binds to activated IRF3 and IRF7 in the nucleus, leading to the inhibition of IFN transcription (50).

The SAP domain binds to AT-rich DNA sequences present in the scaffold attachment regions/matrix attachment regions (51). This domain is conserved in all PIAS members and shown to be required for the interaction with nuclear receptors and their co-regulators (52). We show that the mutant PIASy with an altered L*XX*LL motif in the SAP domain, although unable to inhibit IFN-stimulated ISG transcription, nevertheless retained the ability to inhibit type I IFN transcription. Our results illustrate that PIASy employs different mechanisms to inhibit virus-mediated IFN induction and IFN-stimulated ISG expression. This dichotomy may be accounted for by the difference in the transcriptional pathways by which virus-induced IFN transcription and IFN-stimulated transcription is controlled, namely the former is triggered by the TLR/RLR pathway leading to the activation of IRF3 and IRF7, and the latter is activated by the JAK/STAT pathway activating STAT1/STAT2 and IRF9. In this scenario, PIASy may select SAP-dependent and -independent processes according to the types of transcription factors activated and recruited to the promoter. The significance of the differential domain usage is at present unclear. However, it seems clear that PIASy by adopting diverse mechanisms governs specificity, magnitude, and timing of antiviral effects, thereby fine-tuning innate immunity.

PIAS1 and PIASy do not inhibit expression of all ISGs (21, 36, 37). It is likely that ISGs are divided into distinct groups, partly according to different types of negative regulation under which they are controlled. Because IRF3 and IRF7 are involved not only in type I IFN transcription, but TLR/RLR-mediated ISG induction, the mechanism observed in this study likely contributes to negative regulation of ISG transcription. SAP domain independent inhibition of ISRE activity by PIASy is likely to operate in a relatively early stage of virus infection, prior to the

FIGURE 5. **C-terminal region of PIASy contributes to the inhibition of IRF3- and IRF7-mediated transcription.** *A,* schematic structure of PIAS proteins. Conserved SAP domain, PINIT domain, RING-like domain (*RLD*), acidic domain (*AD*), and serine/threonine-rich domain (*S/T*) are shown on *top*. A series of PIASy C-terminal deletion mutants are shown. *B,* 293T cells were transfected with VISA (*top*) or TRIF (*bottom*), IFNβ promoter reporter, and increasing doses of WT or indicated PIASy mutant. Luciferase activities were quantified by normalizing with *Renilla* luciferase activities. *C,* structure of the C-terminal region of PIASy. Deletion mutants in *B* are shown on *top*. The SIM, CK2 target motif, and acidic domain are *underlined*. Alignment of SIM and CK2 target consensus motif is indicated in the *middle*. Mutants with disrupted SIM and CK2 consensus motifs are on the *bottom*. *D,* HA-tagged WT or mutant PIASy were transfected to 293T cells with or without T7-SUMO1/GA, and extracts were immunoprecipitated (*IP*) with anti-T7 antibody. Immunoprecipitated (*top panel*) and whole cell extracts (*WCE, lower panels*) were analyzed by Western blot (*WB*) with the indicated antibodies. *E,* PIASy$^{-/-}$ MEF expressing WT or indicated PIASy mutants were infected with VSV.IFNβ (*left panel*) and IFNα4 (*right panel*) mRNA at indicated time post-infection (*p.i.*) were quantified by qRT-PCR and by normalizing with hypoxanthine-guanine phosphoribosyltransferase mRNA. The values represent the average of three samples ± S.D. *F,* whole cell extracts in *E* were tested for Western blot (*WB*) with the indicated antibodies. *G,* 293T cells were transfected with VISA (*left panel*) or TRIF (*right panel*) and IFNβ promoter reporter and increasing amounts of WT or indicated PIASy mutants. Luciferase activities were quantified as in *B*.

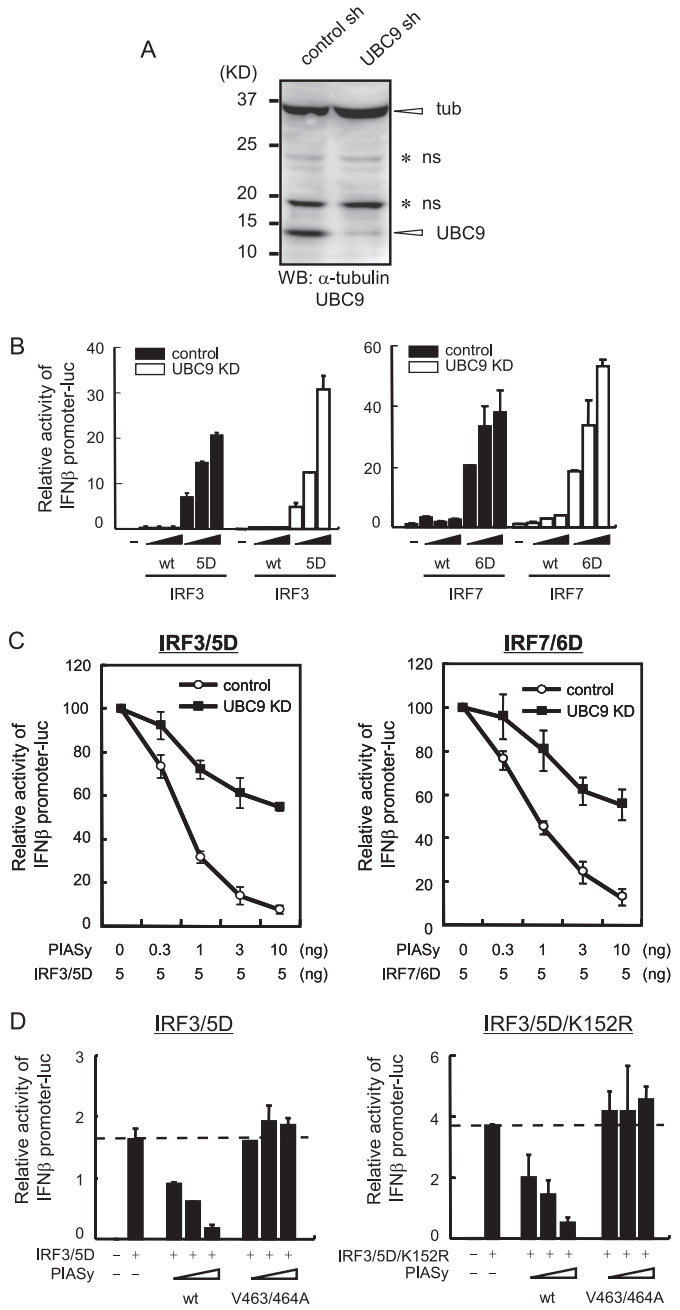

FIGURE 6. **SUMO modification is required for inhibition of type I IFN induction by PIASy.** *A,* whole cell extracts from control or UBC9 knockdown (KD) 293T cells were analyzed by Western blot (*WB*) with the indicated antibodies. UBC9, α-tubulin (*tub*) and nonspecific bands (*ns*) are marked on the *right*. *B,* UBC9 KD or control 293T cells were transfected with WT or the activated form of IRF3 (*left panel*) or IRF7 (*right panel*) and IFNβ promoter reporter. Luciferase activities were quantified by normalizing with *Renilla* luciferase activities. *C,* UBC9 KD or control 293T cells were transfected with the activated form of IRF3 (*left panel*) or IRF7 (*right panel*) and IFNβ promoter reporter and increasing doses of PIASy. Luciferase activities were quantified as in *B*. The promoter activities are expressed as the ratio of PIASy-transfected *versus* untransfected cells. *D,* 293T cells were transfected with IRF3/5D (*left panel*) or IRF3/5D/K152R (*right panel*), IFNβ promoter reporter, and increasing doses of PIASy. Luciferase activities were quantified as in *B*.

initiation of IFN feedback-based ISG expression (46–48). In a later stage of virus infection, ISG expression is boosted by type I IFN induced through the JAK/STAT pathway, controlled by cooperation of PIAS1 and PIASy (37).

Inhibitory activity of PIAS1 is regulated by a phosphorylation-dependent switch by activated IKKα (53). This mechanism is not likely to apply to PIASy given that PIASy does not have a corresponding phosphorylation target. Interestingly, we observed that virus infection induced a slowly migrating band in PIASy Phos-tag PAGE analysis, indicating that PIASy is also phosphorylated during virus infection (data not shown). Although residues targeted for phosphorylation and the kinase that phosphorylates PIASy have not been identified, it is possible that PIASy is activated upon virus and/or IFN induction through phosphorylation.

In addition to SAP domain-independent inhibition, PIASy inhibition of type I IFN transcription did not require its SUMO E3 ligase activity, because the mutation in the RING-like domain did not abolish IRF3- and IRF7-mediated IFN promoter activity. Some transcription factors are known to be regulated by PIASy via SUMO-independent mechanisms (19, 20). For example, PIASy suppresses LEF1-mediated transcription by recruiting LEF1 to the promyelocytic leukemia protein nuclear body (54). Furthermore, PIASy is reported to recruit HDAC1 and HDAC2 without involving its SUMO E3 activity in Smad4 and androgen receptor-mediated transcription (55, 56). These reports, combined with our observation, further support the view that PIASy utilizes varying mechanisms to repress transcription, depending on the signaling pathways activated and the availability of molecules with which it cooperates.

We show that deletion of the acidic cluster juxtaposed with the hydrophobic SIM core resulted in the loss of PIASy function, leading to the loss of inhibition of IFN transcription. The loss of inhibitory activity coincided with the loss of SUMO peptide binding activity. Furthermore, the SIM sequence was required for the inhibition of IFNβ promoter activity. Thus the acidic cluster may confer SUMO binding activity upon PIASy, playing an important role in inhibiting type I IFN induction. On the other hand, serine residues presumed to be phosphorylated by CK2 were dispensable for inhibition of IFN promoter activity (49). Consistent with these data, treatment of CK2 inhibitors, TBB or emodin, did not change PIASy inhibition of IFNβ promoter activity (data not shown). These results suggest that phosphorylation of PIASy, possibly targeted by CK2, is not required for SUMO binding activity of the SIM, although it may be dependent on the acidic cluster (34). There are five consecutive serine residues between the SIM and the acidic cluster in PIASy, and three serine residues are present in the corresponding region of other PIAS members (Fig. 5*C*). The discrepancy on the requirement of CK2-dependent phosphorylation for the SIM activation among PIAS1, PIAS3, and PIASy may be due to a structural difference caused by these residues. PIASy may have a unique mode of SIM activation, different from that utilized by other PIAS proteins. Given that intact SUMO binding activity appears to be required, the SUMO modification mechanism is expected to play a critical role in negative regulation of type I IFN transcription, despite that the PIASy SUMO E3 ligase domain is dispensable. The role for the SUMOylation machinery in PIASy inhibition of IFN transcription is supported by our data that general down-regulation of SUMO conjugation pathways by UBC9 knockdown led to a profound reduction in the inhibitory effect of PIASy. Our results indicate

that PIASy inhibits IRF3- and IRF7-mediated IFN transcription by associating with a factor yet to be unraveled that is conjugated to SUMO. Because SUMOylation of IRF3 was not required for inhibition by PIASy, IRF3 (and presumably IRF7) is not the factor required for SIM binding. The interaction of this unidentified factor may facilitate the formation of a repressor complex. Identification of a PIASy-interacting partner(s) that is modified by SUMO would thus advance our understanding of the mechanism by which PIASy inhibits type I IFN transcription.

In summary, this work shows that among PIAS family members PIASy is the major negative regulator of type I IFN transcription. It inhibits IFN transcription by mobilizing a SUMO modification mechanism through the SIM domain, without relying on its SUMO E3 ligase activity.

Acknowledgments—We thank Dr. Ke Shuai (UCLA) for kindly providing PIASy$^{-/-}$ MEF, Dr. Takashi Fujita for the FLAG-RIG-IN and IFNβ promoter-luciferase plasmids, and Dr. Rongtuan Lin for the FLAG-TRIF, FLAG-IKKε, FLAG-TKB1, and IFNα1 promoter-luciferase plasmids.

REFERENCES

1. Akira, S., Uematsu, S., and Takeuchi, O. (2006) *Cell* **124,** 783–801
2. Kato, H., Takeuchi, O., Sato, S., Yoneyama, M., Yamamoto, M., Matsui, K., Uematsu, S., Jung, A., Kawai, T., Ishii, K. J., Yamaguchi, O., Otsu, K., Tsujimura, T., Koh, C. S., Reis e Sousa, C., Matsuura, Y., Fujita, T., and Akira, S. (2006) *Nature* **441,** 101–105
3. Takeda, K., and Akira, S. (2005) *Int. Immunol.* **17,** 1–14
4. Andrejeva, J., Childs, K. S., Young, D. F., Carlos, T. S., Stock, N., Goodbourn, S., and Randall, R. E. (2004) *Proc. Natl. Acad. Sci. U.S.A.* **101,** 17264–17269
5. Kawai, T., and Akira, S. (2006) *Nat. Immunol.* **7,** 131–137
6. Yoneyama, M., and Fujita, T. (2009) *Immunol. Rev.* **227,** 54–65
7. Yoneyama, M., Kikuchi, M., Natsukawa, T., Shinobu, N., Imaizumi, T., Miyagishi, M., Taira, K., Akira, S., and Fujita, T. (2004) *Nat. Immunol.* **5,** 730–737
8. Hiscott, J., Lin, R., Nakhaei, P., and Paz, S. (2006) *Trends Mol. Med.* **12,** 53–56
9. Durbin, J. E., Fernandez-Sesma, A., Lee, C. K., Rao, T. D., Frey, A. B., Moran, T. M., Vukmanovic, S., García-Sastre, A., and Levy, D. E. (2000) *J. Immunol.* **164,** 4220–4228
10. Hengel, H., Koszinowski, U. H., and Conzelmann, K. K. (2005) *Trends Immunol.* **26,** 396–401
11. Levy, D. E., and García-Sastre, A. (2001) *Cytokine Growth Factor Rev.* **12,** 143–156
12. McGettrick, A. F., and O'Neill, L. A. (2010) *Curr. Opin. Immunol.* **22,** 20–27
13. Moore, C. B., and Ting, J. P. (2008) *Immunity* **28,** 735–739
14. O'Neill, L. A. (2008) *Immunity* **29,** 12–20
15. Komuro, A., Bamming, D., and Horvath, C. M. (2008) *Cytokine* **43,** 350–358
16. Wang, J., Hu, Y., Deng, W. W., and Sun, B. (2009) *Microbes Infect.* **11,** 321–327
17. Rytinki, M. M., Kaikkonen, S., Pehkonen, P., Jääskeläinen, T., and Palvimo, J. J. (2009) *Cell. Mol. Life Sci.* **66,** 3029–3041
18. Schmidt, D., and Müller, S. (2003) *Cell. Mol. Life Sci.* **60,** 2561–2574
19. Sharrocks, A. D. (2006) *Genes Dev.* **20,** 754–758
20. Shuai, K. (2006) *Cell Res.* **16,** 196–202
21. Shuai, K., and Liu, B. (2005) *Nat. Rev. Immunol.* **5,** 593–605
22. Arora, T., Liu, B., He, H., Kim, J., Murphy, T. L., Murphy, K. M., Modlin, R. L., and Shuai, K. (2003) *J. Biol. Chem.* **278,** 21327–21330
23. Chung, C. D., Liao, J., Liu, B., Rao, X., Jay, P., Berta, P., and Shuai, K. (1997) *Science* **278,** 1803–1805
24. Liu, B., Liao, J., Rao, X., Kushner, S. A., Chung, C. D., Chang, D. D., and Shuai, K. (1998) *Proc. Natl. Acad. Sci. U.S.A.* **95,** 10626–10631
25. Liao, J., Fu, Y., and Shuai, K. (2000) *Proc. Natl. Acad. Sci. U.S.A.* **97,** 5267–5272
26. Verger, A., Perdomo, J., and Crossley, M. (2003) *EMBO Rep.* **4,** 137–142
27. Gill, G. (2003) *Curr. Opin. Genet. Dev.* **13,** 108–113
28. Gill, G. (2005) *Curr. Opin. Genet. Dev.* **15,** 536–541
29. Hay, R. T. (2005) *Mol. Cell* **18,** 1–12
30. Kotaja, N., Karvonen, U., Jänne, O. A., and Palvimo, J. J. (2002) *Mol. Cell. Biol.* **22,** 5222–5234
31. Ouyang, J., Valin, A., and Gill, G. (2009) *Methods Mol. Biol.* **497,** 141–152
32. Jackson, P. K. (2001) *Genes Dev.* **15,** 3053–3058
33. Johnson, E. S., and Gupta, A. A. (2001) *Cell* **106,** 735–744
34. Kerscher, O. (2007) *EMBO Rep.* **8,** 550–555
35. Palvimo, J. J. (2007) *Biochem. Soc. Trans.* **35,** 1405–1408
36. Liu, B., Mink, S., Wong, K. A., Stein, N., Getman, C., Dempsey, P. W., Wu, H., and Shuai, K. (2004) *Nat. Immunol.* **5,** 891–898
37. Tahk, S., Liu, B., Chernishof, V., Wong, K. A., Wu, H., and Shuai, K. (2007) *Proc. Natl. Acad. Sci. U.S.A.* **104,** 11643–11648
38. Liu, B., Yang, R., Wong, K. A., Getman, C., Stein, N., Teitell, M. A., Cheng, G., Wu, H., and Shuai, K. (2005) *Mol. Cell. Biol.* **25,** 1113–1123
39. Liu, B., and Shuai, K. (2008) *Trends Pharmacol. Sci.* **29,** 505–509
40. Kubota, T., Matsuoka, M., Chang, T. H., Tailor, P., Sasaki, T., Tashiro, M., Kato, A., and Ozato, K. (2008) *J. Biol. Chem.* **283,** 25660–25670
41. Akaike, T., Fujii, S., Kato, A., Yoshitake, J., Miyamoto, Y., Sawa, T., Okamoto, S., Suga, M., Asakawa, M., Nagai, Y., and Maeda, H. (2000) *FASEB J.* **14,** 1447–1454
42. Sakai, Y., Kiyotani, K., Fukumura, M., Asakawa, M., Kato, A., Shioda, T., Yoshida, T., Tanaka, A., Hasegawa, M., and Nagai, Y. (1999) *FEBS Lett.* **456,** 221–226
43. Zhao, T., Yang, L., Sun, Q., Arguello, M., Ballard, D. W., Hiscott, J., and Lin, R. (2007) *Nat. Immunol.* **8,** 592–600
44. Honda, K., and Taniguchi, T. (2006) *Nat. Rev. Immunol.* **6,** 644–658
45. Liu, B., Gross, M., ten Hoeve, J., and Shuai, K. (2001) *Proc. Natl. Acad. Sci. U.S.A.* **98,** 3203–3207
46. Honda, K., Yanai, H., Takaoka, A., and Taniguchi, T. (2005) *Int. Immunol.* **17,** 1367–1378
47. Marié, I., Durbin, J. E., and Levy, D. E. (1998) *EMBO J.* **17,** 6660–6669
48. Sato, M., Suemori, H., Hata, N., Asagiri, M., Ogasawara, K., Nakao, K., Nakaya, T., Katsuki, M., Noguchi, S., Tanaka, N., and Taniguchi, T. (2000) *Immunity* **13,** 539–548
49. Stehmeier, P., and Muller, S. (2009) *Mol. Cell* **33,** 400–409
50. Zhang, J., Xu, L. G., Han, K. J., Wei, X., and Shu, H. B. (2004) *FEBS Lett.* **570,** 97–101
51. Kipp, M., Göhring, F., Ostendorp, T., van Drunen, C. M., van Driel, R., Przybylski, M., and Fackelmayer, F. O. (2000) *Mol. Cell. Biol.* **20,** 7480–7489
52. Glass, C. K., and Rosenfeld, M. G. (2000) *Genes Dev.* **14,** 121–141
53. Liu, B., Yang, Y., Chernishof, V., Loo, R. R., Jang, H., Tahk, S., Yang, R., Mink, S., Shultz, D., Bellone, C. J., Loo, J. A., and Shuai, K. (2007) *Cell* **129,** 903–914
54. Sachdev, S., Bruhn, L., Sieber, H., Pichler, A., Melchior, F., and Grosschedl, R. (2001) *Genes Dev.* **15,** 3088–3103
55. Gross, M., Yang, R., Top, I., Gasper, C., and Shuai, K. (2004) *Oncogene* **23,** 3059–3066
56. Long, J., Matsuura, I., He, D., Wang, G., Shuai, K., and Liu, F. (2003) *Proc. Natl. Acad. Sci. U.S.A.* **100,** 9791–9796